

# Performance Enhancement of a Variable Speed Permanent Magnet Synchronous Generator Used for Renewable Energy Application

Rasha A. Mohamed<sup>a,1,\*</sup>, Mahmoud A. Mossa<sup>b,2</sup>, Ahmed A. M. El-Gaafary<sup>b,3</sup>

<sup>a</sup>Electrical Engineering Department, Faculty of Engineering, Minia University, Minia 61111, Egypt

<sup>1</sup>[rashaabdelazem2016@gmail.com](mailto:rashaabdelazem2016@gmail.com); <sup>2</sup>[mahmoud\\_a\\_mossa@mu.edu.eg](mailto:mahmoud_a_mossa@mu.edu.eg); <sup>3</sup>[elgaafary@mu.edu.eg](mailto:elgaafary@mu.edu.eg)

\* Corresponding Author

## ARTICLE INFO

## ABSTRACT

### Article history

Received May 11, 2023

Revised July 16, 2023

Accepted July 29, 2023

### Keywords

PMSG;

Wind Turbine;

Ripples;

Predictive Torque Control;

Predictive Power Control;

MPPT;

Current Harmonics

The paper aims to develop an improved control system to enhance the dynamics of a permanent magnet synchronous generator (PMSG) operating at varying speeds. The generator dynamics are evaluated based on lowering current, power, and torque ripples to validate the effectiveness of the proposed control system. The adopted controllers include the model predictive power control (MPPC), model predictive torque control (MPTC), and the designed predictive voltage control (PVC). MPPC seeks to regulate the active and reactive power, while MPTC regulates the torque and flux. MPPC and MPTC have several drawbacks, like high ripple, high load commutation, and using a weighting factor in their cost functions. The methodology of designed predictive voltage comes to eliminate these drawbacks by managing the direct voltage by utilizing the deadbeat and finite control set FCS principle, which uses a simple cost function without needing any weighting factor for equilibrium error issues. The results demonstrate several advantages of the proposed PVC technique, including faster dynamic response, simplified control structure, reduced ripples, lower current harmonics, and decreased computational requirements when compared to the MPPC and MPTC methods. Additionally, the study considers the integration of blade pitch angle and maximum power point tracking (MPPT) controls, which limit wind energy utilization when the generator speed exceeds its rated speed and maximize wind energy extraction during wind scarcity. In summary, the proposed PVC enhanced control system exhibits superior performance in terms of dynamic response, control simplicity, current quality, and computational efficiency when compared to alternative methods.

This is an open-access article under the [CC-BY-SA](https://creativecommons.org/licenses/by-sa/4.0/) license.



## 1. Introduction

Solar, wind, hydro, geothermal, tidal, and wave energy applications have emerged as new models for achieving our civilization's energy requirements [1][2]. Renewable energy sources, unlike fossil fuels, are clean, abundant, naturally replenished, accessible to everyone, and have little or no effect on the environment, so renewable energy production has grown rapidly in recent decades. In terms of the various types of renewable energy resources, wind energy is considered the type that has grown as a result of technological developments, cost reductions, and public demand

for clean energy [3][4]. It competes not only with other renewable energy sources but also with traditional fossil fuel-based power generation units, which cause a lot of damage to the environment, such as higher Carbon dioxide emissions which are considered the main factor in changing the climate [5][6][7], environmental pollutions, so all factors contribute to the selection of wind energy as a renewable energy application [8].

Wind turbines are designed to operate at fixed or variable speeds. Fixed-speed wind turbines (FSWT) use asynchronous generators with a directly coupled three-phase grid to convert the wind energy to electrical energy, which makes it simpler and less costly due to avoiding using power converters. However, FSWT has several disadvantages, such as higher mechanical stress and less efficiency [9] due to producing output turbine power ( $P_{tp}$ ) is less, which is referred to as decreasing power coefficient as increasing  $\lambda_t$  at a constant speed of rotor speed according to the equation of tip speed ratio (TSR) [10]. Variable-speed wind turbines (VSWT) usually use synchronous generators with indirect coupling with the grid through using a power converter, leading to a higher initial cost than (FSWT) [11]. However, the high energy production of VSWTs makes up for their high initial cost. VSWT has many advantages, for example, if the Wind turbine may speed up or slow down. As a result, the tower, gearbox, and other drive train parts will see reduced wear and stress. Additionally, variable-speed devices can boost energy production, which as a result, generates higher power due to the turbine always running at an optimal TSR ratio. Consequently, the power coefficient  $C_p$  value is kept at maximum value, and  $P_{tp}$  always has a cubic relationship with wind speed in comparison with that of fixed speed type. Accordingly, blade angle and MPPT controls should usually be considered with wind-driven generators. And also lessen power injection fluctuation into the grid [12]. All these elements contribute to choosing the variable speed wind turbine.

Asynchronous and synchronous generators are generally used with wind generation systems [13]. An asynchronous type like squirrel cage induction generator (SCIG) is considered the first type used due to its directed connection to the grid and operating at an almost fixed speed [14]. However, its needing a capacitor bank to feed it with reactive power is the main challenge. Another type of asynchronous is the doubly-fed induction generator (DFIG) which has several advantages over squirrel cage induction generator (SCIG), such as handling high-power rating [15], DFIG can be controlled from the stator side or rotor side, but the controlling of DFIG from the rotor side is preferred owing to using low scale converter consequently saving in cost [16][17][18]. Because of the drawbacks of DFIG generators, such as low efficiency, low power factors, needing to slip rings which is the main factor in increasing maintenance processes, and the need for excitation current for the rotor [19][20], so synchronous generators become widely used in wind turbines, especially permanent-magnet synchronous generators (PMSG). The PMSG has many features, like self-excitation, so it operates at a high-power factor, and its efficiency will increase; furthermore, PMSG doesn't use brushes or slip rings for the rotor, which saves maintenance costs. Additionally, the PMSG can couple to the turbine via a gearbox or directly without a gearbox which reduces the weight of the nacelle and also lower operating noise due to using permanent magnets in the rotors [21][22][23].

Many types of control methods can be applied for generators, but choosing the most appropriate control is one of the most challenging points in the generation system. Field-oriented control (FOC) and direct torque control (DTC) are considered the most commonly used strategies for the control of PMSMs owing to simple implementation [24][25]. FOC independently manages active and reactive or torque and flux by utilizing two separate inner current loops (PI), which proved its ability to control nonlinearities in the generator model, reducing ripples and having a smooth dynamic response. On the other hand, the complexity due to using the coordinate transformation, delay response, and its dependence on the machine parameters as the result of using the PI is still significant defects of using FOC. An attempt to avoid the shortcomings of FOC is DTC which replaced the PI controls with hysteresis comparators. DTC has several advantages such as simple implementation and no need to coordinate transformation, fast dynamic response, and less

computation effort compared with the FOC [26], but it suffers from high current and torque ripple due to using the hysteresis compactors compared to DTC. Another approach that follows the same principle of DTC is direct Power Control (DPC) which controls active and reactive powers [27][28]. Due to the existing relationship between the active power and developed torque, so controlling the active power results in controlling on developed torque, while controlling reactive power results in controlling the flux. Consequently, DPC is considered a transformation of the DTC strategy [29][30].

Recently, many advanced control strategies appeared to eliminate the shortcomings of FOC, DTC, and DPC especially significant sensitivity as a result of the presence of torque ripples and the dependence on generator parameters. It is generally known that nonlinear controls are less sensitive to system parameters. For this reason, Numerous studies examined these techniques, such as sliding mode control (SMC) and Model predictive control (MPC). Sliding mode control is a nonlinear control, so it is a more suitable technique for dealing with disturbances. SMC has several features such as good dynamic response, high robustness against parameters variations compared to FOC, low ripple compared to DTC and DPC, and simple implementation in addition to the ability to deal with any existing disturbance or unmolded dynamics [31][32][33]. However, some drawbacks appear as the chattering phenomena and reaching phase stability problems [34].

Another attempt to deal with nonlinearities is Model predictive control (MPC) to address the flaws of FOC, DTC, and DPC, which predicts the plant's future behavior and implements the optimal control actions according to the predefined control objectives. MPC has several advantages. For instance, simple to apply to a multivariable system and give a fast dynamic response in addition to the ability to include control loops in one loop. Furthermore, it makes it simple to add nonlinearities and limitations to the control rule [35]. Nowadays, MPC is becoming one of the popular techniques that are classified into two topologies [15]. The first type is MPC with a modulator such as that predictive control that replaced the PI regulator with a cost function and used a modulator, whatever its type, PWM or SVPWM, to generate the signal to the converter control. As a result, this type has a constant frequency switching operation. However, due to using the modulator and depending on system models so this type becomes very sensitive to uncertainties. The second type is MPC without modulation, such as finite set control (FSC-MPC), which doesn't need to use any modulator or PI regulator. This makes the switching frequency variable, in addition to choosing the most appropriate voltage from a set of eight vectors [36][37]. The FSC-MPC needs to predict the reference value from instant  $k$  to  $k + 1$  sampling instant and the predictive module to get the predictive value and, finally, cost function to evaluate the prediction and provide the signals because of the flexibility that appeared in using the cost function in FSC-MPC, which offers more flexible criteria for choosing optimal switching signals and the ability to include multi-objective control requirements (such as system nonlinearities and limits), and fast dynamic response. These factors lead to the usage of the FSC principle with various predictive controllers for the PMSG, such as FSC-MPPC and FSC-MPTC. The above information can be clarified by looking at the design of the FCS-MPC techniques that are being employed, in which the look-up tables and hysteresis regulators disappear as in MP DTC, or the PI current and power regulators are eliminated as in MP PC by using an only cost function. All of this has effectively reduced system complexity, which has sped up system dynamics.

In [38], MPPC employed the same concept as traditional DPC, but instead of using hysteresis and a lookup table, it used a cost function to decrease the errors between active and reactive powers. In [39], MPPC replaced the using multiple PI regulators and modulators in SVOC by using the cost function to achieve simplicity. MPPC has several merits, such as good dynamic response, Simple implementation. On the other hand, Big control variable ripples are characterized by one switching vector per control interval is still the main problem in addition to using the weighting factor ( $W_i$ ) to fulfill the balance between its absolute errors variable due to its nature being different for example in [17], the cost function is the absolute errors between the reference and estimated values of real and reactive powers. Both active and reactive powers have different orders of magnitude, so their errors

aren't equalled, and accordingly, the weighting factor is an important factor in achieving the balance between the active and reactive powers. To determine this value, a trial-and-error concept is considered. In the same manner, MPTC is considered an attempt to maintain the simplicity and reduce the ripple in traditional DTC by replacing or eliminating the hysteresis and look-up table with a more flexible cost function that includes the errors between the torque and flux and multiplied by a weighting factor ( $W_f$ ). The MPTC has several demerits such that the calculation burden is increased due to the need to estimate and predict values of the torque and flux in the cost function, consequently, needing a high microprocessor is very necessary for this defect [40]. This means long sampling intervals and low switching frequency, leading to an increase in the torque ripple and reducing the quality of the generated stator currents and using the weighting factor. In [41], by forecasting the torque and stator flux magnitude on the stationary reference frame instead of the synchronously rotating reference frame, it is intended to prevent using a weighting factor. A new cost function based on the reactive torque and active torque components is also created to reduce the capacity of calculations [42][43]. Due to the equal size of the reactive and active torques, the weighting element necessary in the traditional MPTC system is removed. However, the computational burden is still affected. Another attempt to eliminate using a weighting factor in the cost function is the MPCC approach which makes it simpler than SVOC and MPTC, in addition to the reduction of the ripple in torque and flux as in both MP TC and MPPC strategies. MPCC is considered a transport of FOC. In MPCC, we replace the PI current in FOC with a simple cost function that combines the errors between the direct and quadrature stator current without using any weighting factor ( $W_f$ ) [44]. However, the drawback of the MPCC is the cost function needs estimating and prediction values, so any change in machine parameters will affect the performance, MPCC achieved simpler constructor and faster dynamics repose than FOC [45].

Many recent researchers have looked to formulate a new cost function in which there is no requirement to use a weighting factor or estimating parameters. Up to this detailed review, we aim to design an effective control for fulfilling these needs and avoiding the drawbacks of traditional MPPC and MPTC approaches, so the present study aims to formulate a predictive control technique that utilizes a unique cost function without using a weighting value and which also doesn't require high computation regime which results in limiting the commutation losses and producing better performance such as fast dynamic response compared to sliding mode control and low ripple compared to model predictive Torque and model predictive power controllers, robust against the parameters variation compared to DTC, FOC, and other classic predictive controllers.

The formulated cost function will consist of the absolute errors between the actual and reference d-q components of stator voltages. The reference voltage signals will be derived systematically depending on the deadbeat control principle; meanwhile, the actual voltage terms are obtained using the finite control set (FSC) principle.

In summary, the paper's contributions are discussed as follows.

- The research develops an efficient predictive voltage control (PVC) strategy that fixes the flaws in earlier PMSG control techniques.
- The paper includes an extensive evaluation of the performance of the PMSG utilizing the developed PVC system and other control methods.
- The paper presents a flow chart of three predictive controls.
- The paper provides a thorough explanation of each of the control strategies that are discussed to illustrate the basic concept behind each approach as well as the advantages and disadvantages.
- The results ensure and prove that the designed PVC outperforms alternative control schemes in terms of quick dynamic response, simplicity, reduced ripples, less computational load, and robustness against the parameters' variation.

The present study in this article is structured such that in [Sec. II](#), the detailed modeling of all system components is described and the description of wind turbine control. In [Sec. III](#), methods that adopted predictive controllers with the generator side converters and the control of the grid side converter. In [Sec. IV](#), the results obtained using different control algorithms are analyzed, and a detailed comparative study is carried out. Finally, [Sec. V](#) provides the conclusion and outcomes of the study.

## 2. Modeling of System Components

[Fig. 1](#) shows that the system under study consists of a variable wind speed turbine connecting directly with a Permanent synchronous generator, a three-phase rectifier I (MSC), and a three-phase inverter (GSC) linked together through a dc link capacitor and also before connecting the permanent magnet synchronous generator to the grid the filter has been used. For this system, we evaluated the dynamics performance generator under study by using different control strategies to identify the most operating one, which is claimed to be the proposed predictive voltage. To approve these claims, a detailed mathematical model for each system unit must be presented.

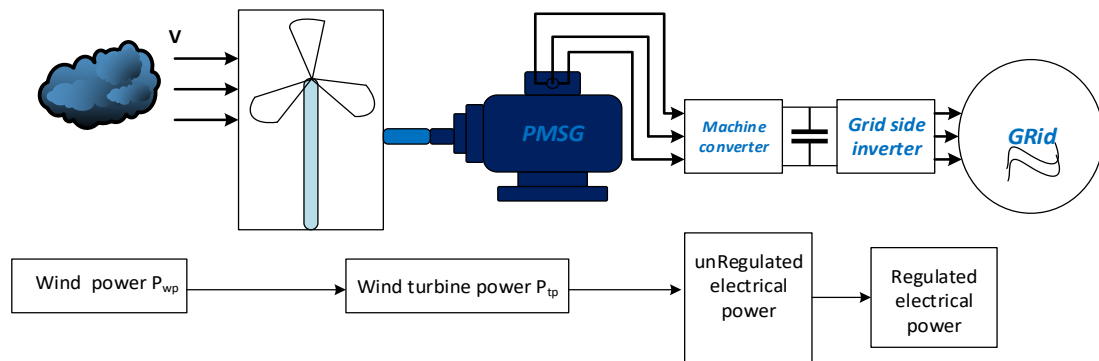


**Fig. 1.** Block schematic of a component system for converting wind kinetic energy into electricity.

### 2.1. Mathematical Model of PMSG

A permanent magnet synchronous generator requires an electromagnetic field with a flexible structure, which results in high standards of operation and manufacturing besides the cost of inverters; however, it is popularly used in variable wind speed turbines due to the advantages we have mentioned before [\[29\]](#). The top one of that is it doesn't need an excitation circuit in the rotor, so it doesn't need slip rings. [Fig. 2](#) depicts the steady-state PMSG model [\[51\]\[10\]](#). Where  $u_{sd}$ ,  $u_{sq}$ ,  $i_{sd}$ ,  $i_{sq}$ ,  $L_d$ ,  $L_q$ ,  $\lambda_{sd}$ ,  $\lambda_{sq}$ ,  $\lambda_{pm}$ ,  $w_e$ ,  $w_g$ , and  $P$  are the direct stator voltage, the quadrature stator voltage, direct stator current, quadrature stator current, direct stator inductance, quadrature stator inductance, direct stator flux, quadrature stator flux, the permanent magnet flux, electrical angular speed, mechanical angular speed and the number of pair pole of PMSG generator in the synchronous rotating d-q reference frame [\[52\]](#).

The dynamic model of PMSG seen in [Fig. 2](#) can be represented at instant  $KT_s$  by using sampling time  $T_s$  as in [\(1\)](#) and [\(2\)](#).

$$\frac{d}{dt} i_{sd,(k)} = \frac{l}{L_d} (u_{sd,(k)} - R_s i_{sd,(k)} + w_{e,(k)} \lambda_{sq,(k)}) \quad (1)$$

$$\frac{d}{dt} i_{sq,(k)} = \frac{l}{L_q} (u_{sq,(k)} - R_s i_{sq,(k)} - w_{e,(k)} \lambda_{sd,(k)}) \quad (2)$$

From [\(1\)](#) and [\(2\)](#), where  $\lambda_{sd,(k)}$  and  $\lambda_{sq,(k)}$  are  $d$  and  $q$  stator flux in a synchronous reference frame which is obtained by [\(3\)](#) and [\(4\)](#).

$$\lambda_{sd,(k)} = L_d i_{ds,(k)} + \lambda_{pm,(k)} \quad (3)$$

$$\lambda_{sq,(k)} = L_q i_{qs,(k)} \quad (4)$$

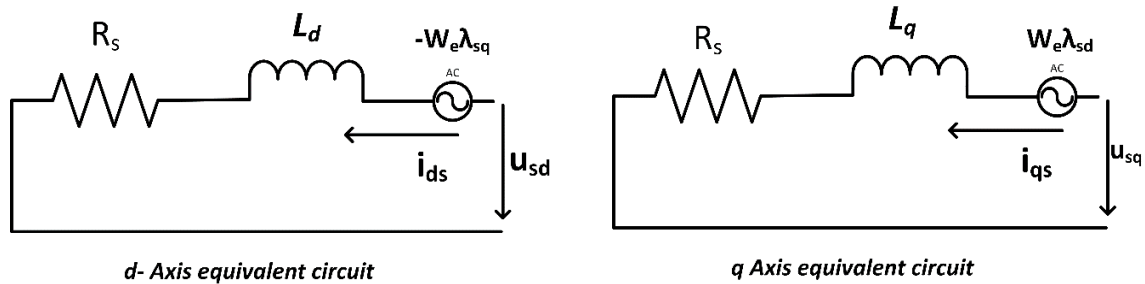


Fig. 2.  $d - q$  axis PMSG model

As seen below, there exists a relationship between electrical and mechanical angular speeds given by (5).

$$w_{e,(k)} = P w_{g,(k)} \quad (5)$$

By using (3), (4), and (5), the electric dynamics of PMSG can be described by (6) and (7).

$$\frac{d}{dt} i_{sd,(k)} = \frac{l}{L_d} (u_{sd,(k)} - R_s i_{sd,(k)} + L_{sq} P w_{g,(k)} i_{sq,(k)}) \quad (6)$$

$$\frac{d}{dt} i_{sq,(k)} = \frac{l}{L_q} (u_{sq,(k)} - R_s i_{sq,(k)} - L_d P w_{g,(k)} i_{sd,(k)} - \lambda_{pm} P w_{g,(k)}) \quad (7)$$

Alternatively, the mechanical dynamics of PMSG are represented by equation (8).

$$\frac{d}{dt} w_{g,(k)} = \frac{1}{j_{eq}} (T_{t,(k)} - T_{e,(k)} - F_r w_{g,(k)}) \quad (8)$$

Where  $j_{eq}$  is equivalent inertia moment of the turbine and generator,  $T_{t,(k)}$  is Turbine torque,  $T_{e,(k)}$  is Electromagnetic torque,  $F_r$  is Friction of the rotor. The permanent magnet flux linkage and stator current components are used to express the electromagnetic torque of the PMSG, which can be stated mathematically as (9).

$$T_{e,(k)} = 1.5P (\lambda_{pm} i_{sq,(k)} + (L_d - L_q) i_{sd,(k)} i_{sq,(k)}) \quad (9)$$

As the inductances on the  $d$  and  $q$  axis are the same ( $L_d = L_q$ ), the electromagnetic torque ( $T_{e,(k)}$ ) can be expressed by (10).

$$T_{e,(k)} = 1.5 p \lambda_{pm} i_{sq,(k)} \quad (10)$$

## 2.2. Wind Turbine Aerodynamic Model

Wind turbines transfer wind energy to mechanical energy. The wind power is calculated as in (11) [46].

$$P_{wp} = 0.5 \rho A V_w^3 \quad (11)$$

Where  $\rho$  the air density [kg/m<sup>3</sup>] is,  $A = \pi r^2$  is the swept area of the wind turbine  $V_w$  is wind speed [m/s] as it isn't possible to catch all the power from the wind, so the turbine power is calculated by (12) [13].

$$P_{tp} = C_p P_{wp} = 0.5 \pi C_p \rho r^2 V_w^3 \quad (12)$$

Where  $C_p$  the power coefficient that controls and regulates how much electricity comes from wind energy. The power coefficient depends on bitch angle  $[\beta]$  and tip ratio speed  $[\lambda_t]$  to get  $C_p$  for given  $\lambda_t$  and  $\beta$ . The following equations have been used for this aim. The power coefficient is calculated by (13) [47][48].

$$C_p(\lambda_t, \beta) = 0.5176 \left( \frac{116}{\lambda_i} - 0.4\beta - 5 \right) e^{-\frac{21}{\lambda_i}} + 0.0068\lambda_t \quad (13)$$

Where  $\lambda_i$  is given by (14).

$$\frac{1}{\lambda_i} = \frac{1}{\lambda_t + 0.08\beta} - \frac{0.035}{1 + \beta^3} \quad (14)$$

The characteristics of the power coefficient ( $C_p$ ) and the tip speed ratio ( $\lambda_t$ ) for different values of bitch angle ( $\beta$ ) are shown in Fig. 3. It is vividly from Fig. 3 we can get the maximum power coefficient when the tip speed ratio reaches the optimum value, and the pitch angle is zero [49][50].

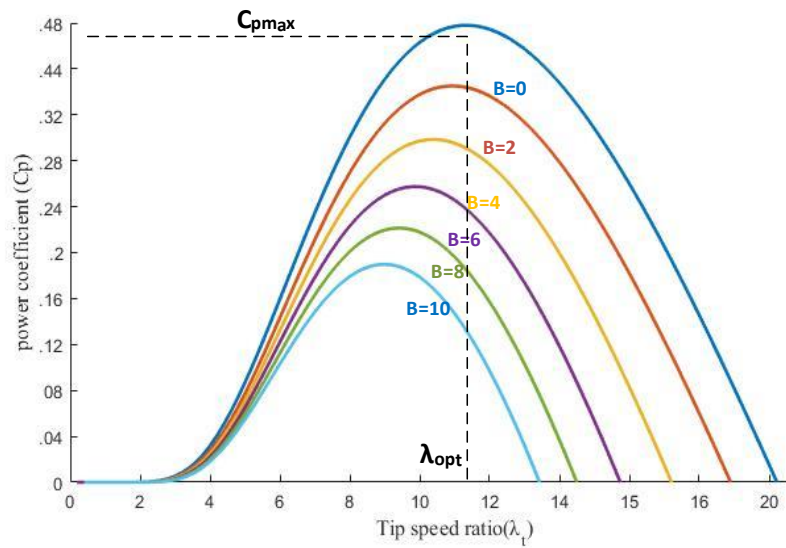


**Fig. 3.** The relationship between power coefficient ( $C_p$ ) and tip speed ratio ( $\lambda_t$ ) for various values of  $\beta$

The tip speed ratio ( $\lambda_t$ ), is obtained by (15) [51].

$$\lambda_t = \frac{w_{g,(K)}r}{V} \quad (15)$$

The mechanical torque or turbine Torque ( $T_t = T_m$ ) is calculated in (16).

$$T_m = T_t = \frac{P_{tp}}{w_{g,(K)}} \quad (16)$$

The mechanically transmitted torque to the generator (generator torque) is evaluated by (17).

$$T_e = T_{w-g} = \frac{T_t}{n_g} \quad (17)$$

Where  $n_g$  is the gearbox ratio and  $w_g$  is the rotor speed. In this paper, PMSG is used without a gearbox, so the gearbox ratio = 1, so the rotor speed, mechanical speed, and generator speed are the same.

### 2.3. MPPT and Pitch Angle Control of Wind Turbine System

Extracting the maximum power from the wind turbine can be achieved by setting the tip ratio speed at its optimum value and the remaining bitch angle at a constant value in the case of low speed

while limiting the machine to operate at the power exceeds its rated power is achieved by the pitch angle control in case over rated speed. This can be accomplished systematically as follows.

#### a. MPPT Operation

It is obvious from Fig. 5 that the MPPT is operated at region (2) only when wind speed is less than the rated value but greater than the cut-in value. The MPPT is a technique to catch maximum power for any given wind. To get the maximum power in this approach, the pitch angle is set to zero degrees, and the turbine works at the optimum speed ratio,  $\lambda_{opt}$ , so the power coefficient  $C_p$  becomes  $C_{pmax}$  by replacing their optimum value in (12), the maximum power is obtained by (18).

$$P_{max} = 0.5\rho C_{pmax} \pi r^2 \left( \frac{w_{g,(K)} r}{\lambda_{opt}} \right)^3 \quad (18)$$

Where the wind speed can be redefined according to (15) as in (19).

$$V_w = \frac{w_{g,(K)} r}{\lambda_{opt}} \quad (19)$$

The maximum power from a wind turbine can be then formulated by (20).

$$P_{max} = k_{opt} (w_{g,(K)})^3 \quad (20)$$

Where  $k_{opt}$  is the coefficient of the wind turbine. The reference speed of a generator can be calculated using the maximum power point tracking of a wind turbine and equation (21).

$$w_{g,(K)}^* = \sqrt[3]{\frac{P_{max}}{k_{opt}}} \quad (21)$$

Referring to (18), the power coefficient reaches its maximum value,  $C_{pmax}$ , if the PMSG velocity can always be regulated to keep the turbine operating under optimum different speed ratio  $\lambda_{opt}$  during variations in wind velocity. That's another way of indicating that the turbine system achieves its maximum power, as shown in Fig. 4. It is remarkable from this figure that, for a given wind speed, the turbine power (mechanical power) changes with generator speed and extracts its maximum value all the time [50].

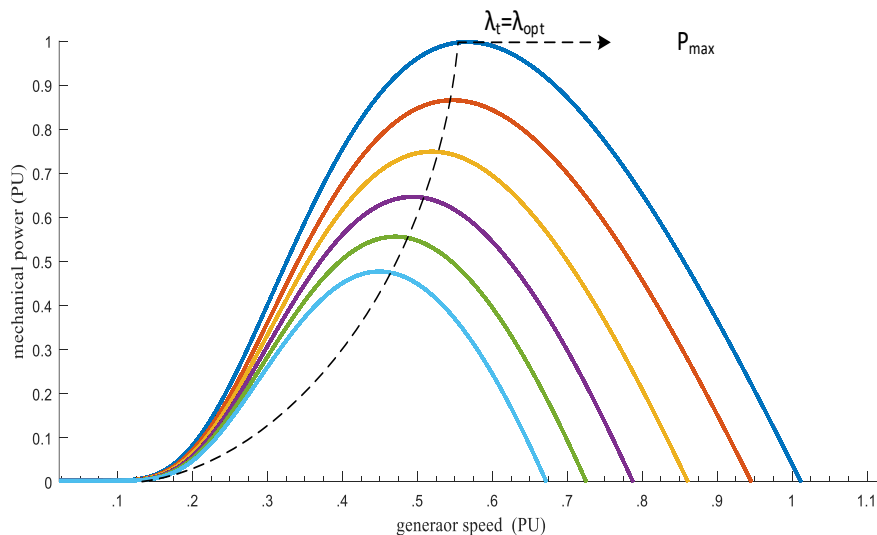


Fig. 4. The relation between the mechanical power and generator speed for various values of wind speed

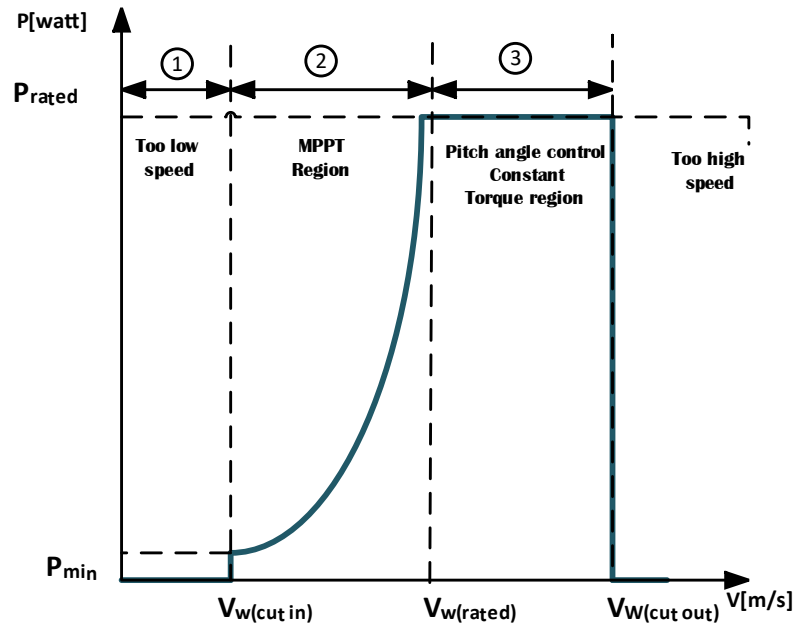


Fig. 5. Operation region of wind turbine

### b. Pitch Angle Control of Wind Turbine

The goal of utilizing pitch angle control is to keep the machine operating at rated output power when wind speed is above its rated. Normally, the pitch angle is set to zero degrees at the MPPT region and activated at the torque region, as in Fig. 5. As a result, the proportional-integral (PI) controller generates  $\beta$  to limit generator output power to its rated value.  $C_p$  drops together with the extracted wind power when the pitch angle increases (refer to (12)), and the generator power returns to its rated value. The schematic of pitch angle control is presented in Fig. 6.

The methodology of using a Pitch angle controller is that the power signals are utilized as the feedback of PI control and the difference between the rated power and the actual power ( $P_e = T_e \times W_e$ ) of the generator is fed to PI, which is responsible for generating maximum power for available wind. While the wind signals for forward control are used (max) for ensuring the activation of the p-angle control only in case the actual wind speed is higher than its rated value [52].

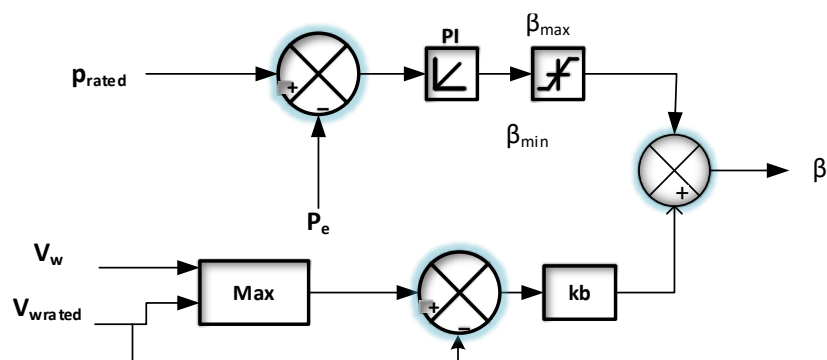


Fig. 6. Pitch angle control

## 3. Methods

This section will represent three different control methods for the machine side converter (MSC), which are MPPC, MPTC, and the proposed PVC scheme. Alternatively, the voltage-oriented control (VOC) algorithm is utilized to manage the grid side converter (GSC) converter.

### 3.1. Grid Side Converter (GSC)

The grid-side electrical circuit equations developed in the synchronous rotating  $d - q$  reference frame can be expressed by (22) and (23).

$$U_{gd} = R_f I_{gd} + L_f \frac{dI_{gd}}{dt} - \omega L_f I_{gq} + V_{gd} \quad (22)$$

$$U_{gq} = R_f I_{gq} + L_f \frac{dI_{gq}}{dt} + \omega L_f I_{gd} + V_{gq} \quad (23)$$

Where  $I_{gd}$ ,  $I_{gq}$ ,  $V_{gd}$ ,  $V_{gq}$ ,  $U_{gd}$ ,  $U_{gq}$  are the grid currents, grid voltages, and voltage at grid side converter output in d-q axis reference frame, respectively.  $R_f$ ,  $L_f$  are the resistance and inductance of the grid filter.

The main objective of using grid-side converter control is to keep the DC link voltage constant [53] during controlling the active ( $P_{gi}$ ) and reactive ( $Q_{gi}$ ) power injected into the grid can be expressed in (24) and (25) [54].

$$P_{gi} = 1.5(V_{gd}I_{gd} + V_{gq}I_{gq}) \quad (24)$$

$$Q_{gi} = 1.5(V_{gq}I_{gd} - V_{gd}I_{gq}) \quad (25)$$

According to the previous equations, in the power terms, the  $d$ -axis and  $q$ -axis components of grid currents and voltages are cross-coupled, making active and reactive power difficult to control.

The VOC control is implemented in this case in the grid voltage synchronous reference frame [13]. The rotating grid voltage space vector is aligned with the d-axis reference frame., and as a result of that, the quadrature grid voltage equals zero. Using the voltage-oriented control technique, the active and reactive power equations can be represented as the following expression. The coupling issue is solved by using the voltage-oriented control method as the grid control, as shown in (26) and (27).

$$P_{gi} = 1.5(V_{gd}I_{gd}) = V_{dc}I_{dc} \quad (26)$$

$$Q_{gi} = 1.5(-V_{gd}I_{gq}) \quad (27)$$

These equations show that the d-axis and q-axis components of grid currents can control active and reactive power independently.

According to the grid scheme in Fig. 7, the VOC needs an outer loop (dc voltage loop) to generate a reference direct grid current for active power, referring to (23) by sending the errors between the measured dc voltage and dc reference to PI control. It also needs an inner current loop to control the reactive power, in addition to removing the current cross-coupling between the d and q components, which necessitates feed-forward compensation of some terms ( $\omega L_f I_{gd}$ ,  $\omega L_f I_{gq}$ ). For the coordinate's transformation, the Phase Locked Loop (PLL) calculates the grid voltage space vector angle. As mentioned earlier, the d-axis of the reference frame is aligned with the grid voltage space vector. The quadrature grid voltage accordingly equals zero. Then, to achieve a unity power factor, the reference of the quadrature grid current is set to zero ( $I_{gq}^* = 0$ ). Finally, the gate drive pulses are obtained through a PWM.

### 3.2. Control of Machine Side Converter (MSC)

The machine-side converter is controlled by three different model predictive methods. The controllers are MPPC and MPTC, and the proposed PVC, which are described in detail to approve the validation of the proposed control.

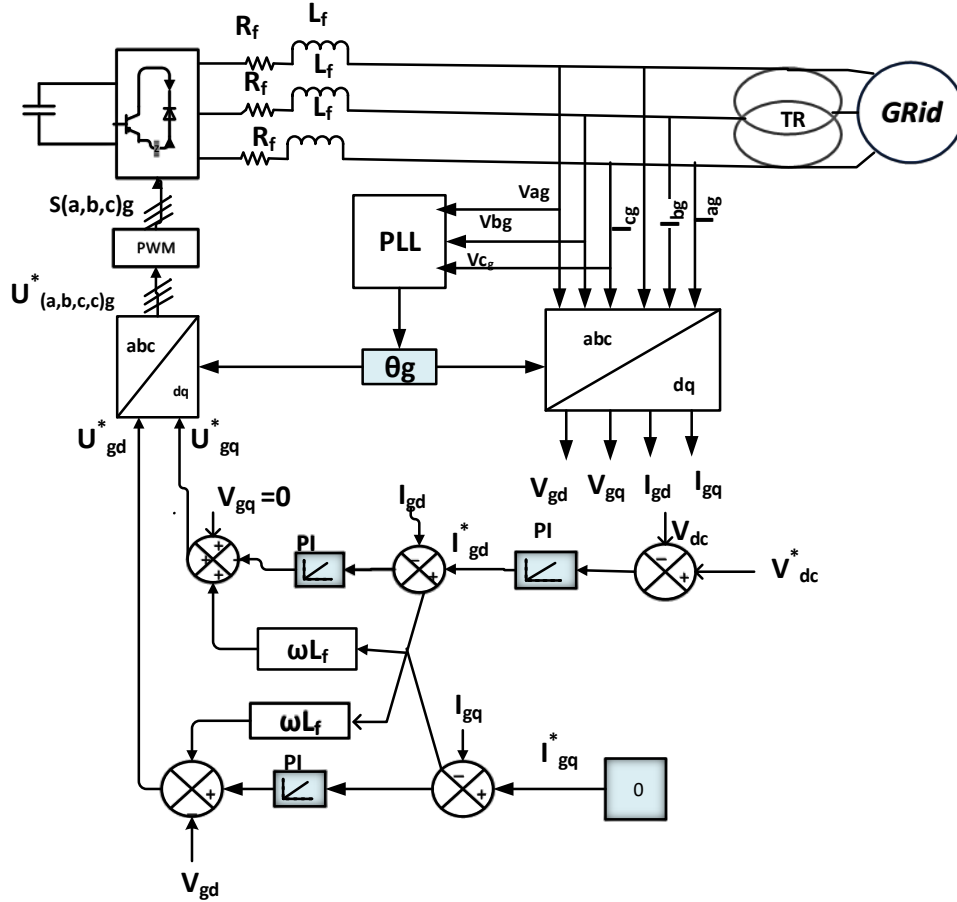


Fig. 7. VOC for grid side Inverter

### a. Model Predictive Power Control (MPPC)

MPPC is aimed to manage stator active and reactive powers directly without using coordinate transformations, linear current controllers or modulators as in stator voltage-oriented control, or torque and flux loops as in MPTC. The cost function (CF) is the main objective of the MPPC, which tries to minimize the absolute errors between the reference and prediction values of stator active and reactive power levels for sending the signal to voltage vector selection to choose the best voltage vector out of a set of vectors (0...7) that achieves this minimization and apply it at the next sample time [38]. The MPPC also uses a weighting value ( $w_v^p$ ), to maintain equilibrium between the controllable powers. The CF used by the MPPC is then expressed by (28).

$$\cap_{k+1}^i = \left| P_{s,(k+1)}^* - P_{s,(k+1)}^p \right|^i + w_v^p \left| Q_{s,(k+1)}^* - Q_{s,(k+1)}^p \right|^i \quad (28)$$

where  $P_{s,(k+1)}^*$ ,  $P_{s,(k+1)}^p$ ,  $Q_{s,(k+1)}^*$ , and  $Q_{s,(k+1)}^p$  are reference stator active power, predictive stator active power, reference stator reactive power, and predictive stator reactive power, respectively, and the superscript  $i$  gives the sectors from 0 to 7.

The reference of active power is generated by multiplying the reference of electromagnetic torque and the mechanical speed ( $w_{g,(k)}^*$ ), which is obtained from MPPT, while the reference of the reactive power ( $Q_{s,(k+1)=0}^*$ ) is set to zero to make the power factor equal to one. Furthermore, the predicted values of active and reactive controlled power are expressed in (29) and (30).

$$P_{s,(k+1)}^p = 1.5(u_{sd,(k+1)}^p i_{sd,(k+1)}^p + u_{sq,(k+1)}^p i_{sq,(k+1)}^p) \quad (29)$$

$$Q_{s,(k+1)}^p = 1.5(u_{sq,(k+1)}^p i_{sd,(k+1)}^p - u_{sd,(k+1)}^p i_{sq,(k+1)}^p) \tag{30}$$

As can be seen from these equations, the stator powers at the next sampling moment rely on the stator direct and quadrature currents at that same instant. So, the prediction of the stator current of  $d - q$  components is obtained by using the forward Euler method as (31) and (32).

$$i_{sd,(k+1)}^p = i_{sd,(k)} + \frac{l}{L_d} (u_{sd,(k)} - R_s i_{sd,(k)} + L_q P W_{g,(k)} i_{sq,(k)}) T_s \tag{31}$$

$$i_{sq,(k+1)}^p = i_{sq,(k)} + (\frac{l}{L_q} (u_{sq,(k)} - R_s i_{sq,(k)} - L_d P W_{g,(k)} i_{sd,(k)} - \lambda_{pm} P W_{g,(k)}) T_s \tag{32}$$

Similarly, the stator voltage components  $u_{sd,(k+1)}^p$  and  $u_{sq,(k+1)}^p$  are obtained as (33) and (34).

$$u_{sd,(k+1)}^p = (\frac{u_{sd,(k)} - u_{sd,(k+1)}}{\Delta T}) T_s \tag{33}$$

$$u_{sq,(k+1)}^p = (\frac{u_{sq,(k)} - u_{sq,(k+1)}}{\Delta T}) T_s \tag{34}$$

Fig. 8 shows the schematic for the MPPC for the MSC. The flow chart is presented in Fig. 9 to display the operation steps of the MPPC, which starts with estimating both the stator current and voltage values and then sampling. After that, the values of the  $dq$  prediction stator current are calculated according to (31) and (32) to compute the prediction values of the active and reactive power through (29) and (30) and also the reference values are measured ending with cost function determination to apply the voltage that gives the minimum value of it.

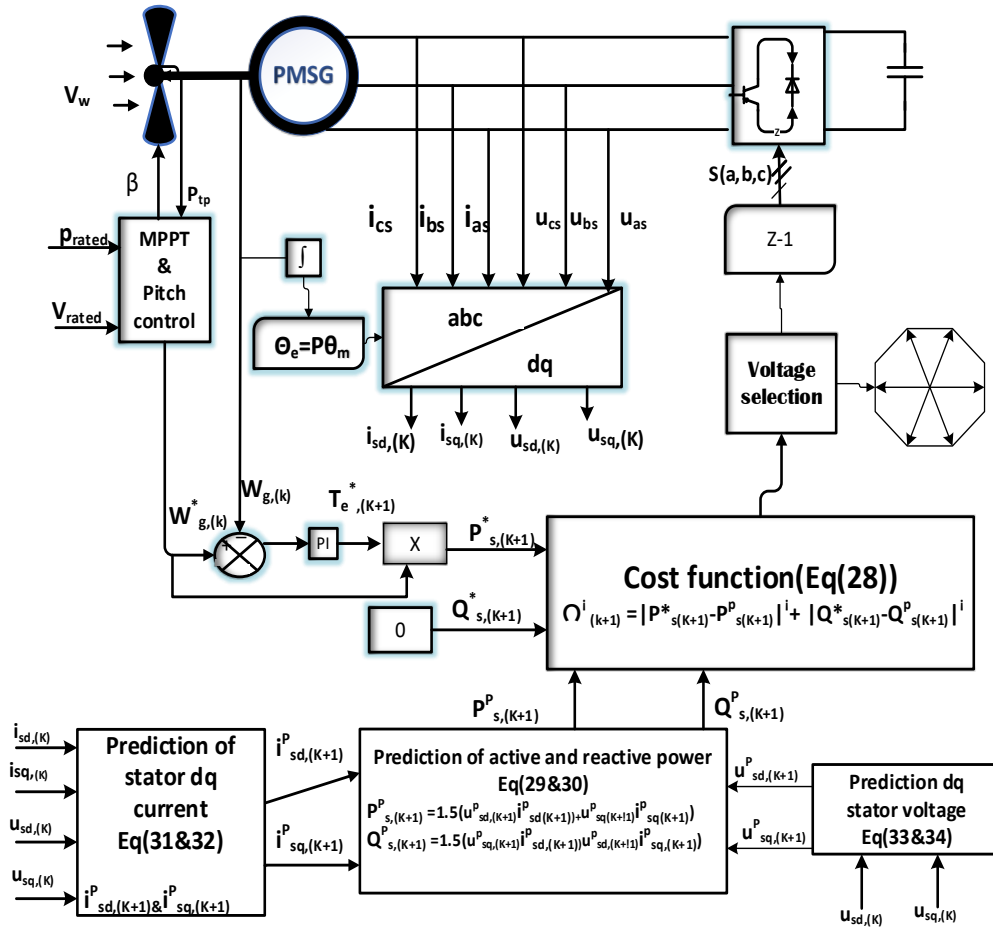


Fig. 8. MPPC for the machine-side converter

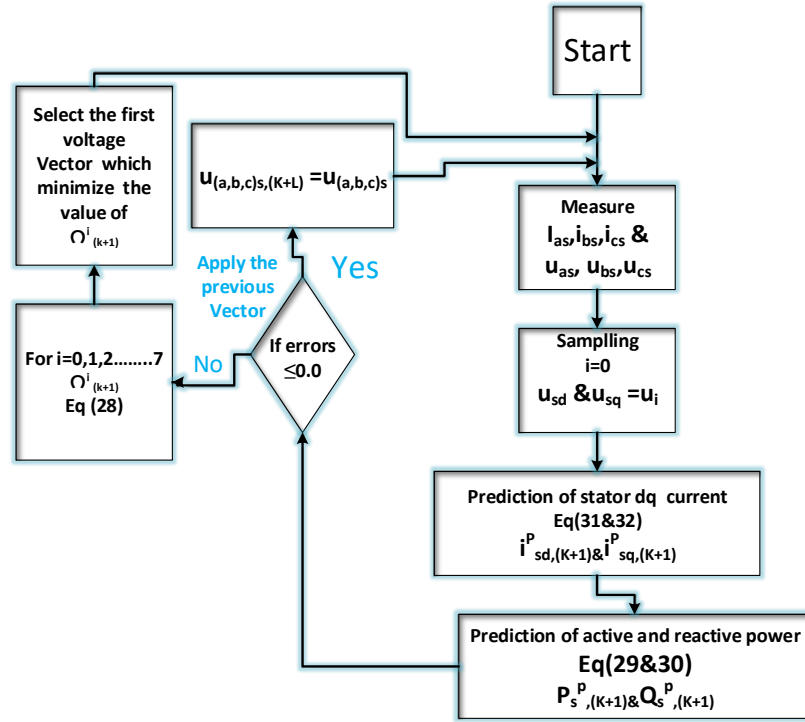


Fig. 9. Flow chart of MPPC for the machine-side converter

### b. Model Predictive Torque Control (MPTC)

The MPTC is responsible for controlling the flux and torque of the PMSG. A cost function reduces the absolute difference between the reference torque and its predictive value and the absolute difference between of reference flux and its predictive value. The cost function also uses a weighting value ( $w_v^t$ ) to fulfill the balance between the torque and flux because of their difference in nature. The look-up tables and hysteresis controllers used in the traditional DTC technique have been replaced with this cost function. In light of this, the cost function of the MPTC [55][56] can be stated by (35).

$$\nabla_{k+1}^i = \left| T_{e,(k+1)}^* - T_{e,(k+1)}^p \right|^i + w_v^t \left| \lambda_{s,(k+1)}^* - \lambda_{s,(k+1)}^p \right|^i \quad (35)$$

Where  $T_{e,(k+1)}^*$ ,  $T_{e,(k+1)}^p$ ,  $\lambda_{s,(k+1)}^*$ , and  $\lambda_{s,(k+1)}^p$  are reference torque, predictive torque, reference stator flux, and predictive stator flux, respectively.

The reference  $T_{e,(k+1)}^*$  is calculated from the wind control but the reference  $\lambda_{s,(k+1)}^*$  is obtained from (36).

$$\lambda_{s,(k+1)}^* = \sqrt{(\lambda_{pm} + L_d i_{sd,(k+1)}^*)^2 + (L_q i_{sq,(k+1)}^*)^2} \quad (36)$$

The permanent magnet can be kept from demagnetizing in interior PMSGs if the  $d$ -axis current is consistently kept at zero, according to (37).

$$i_{sd,(k+1)}^* = 0 \quad (37)$$

According to the previous consideration, the stator flux reference is calculated by (38).

$$\lambda_{s,(k+1)}^* = \sqrt{(\lambda_{pm})^2 + (L_q i_{sq,(k+1)}^*)^2} \quad (38)$$

The reference  $q$ -axis current needed by (38) can be obtained by (39).

$$i_{sq,(k+1)}^* = \frac{T_{e,(k+1)}^*}{1.5 p \lambda_{pm}} \tag{39}$$

The predictive torque and flux in the rotating reference frame at sample time  $(k + 1) Ts$  are given by (40) and (41).

$$T_{e,(k+1)}^p = 1.5 p \lambda_{pm} i_{q_{k+1}}^p \tag{40}$$

$$\lambda_{s,(k+1)}^p = \sqrt{(\lambda_{pm} + L_d i_{d_{k+1}}^p)^2 + (L_q i_{q_{k+1}}^p)^2} \tag{41}$$

Where  $i_{sd,(k+1)}^p$  and  $i_{sq,(k+1)}^p$  are calculated by using (31) and (32).

The schematic of MPTC for the machine side converter is illustrated in Fig. 10, while Fig. 11 presents a flow chart to display the operation steps of the MPTC, in which both stator voltages and stator current are measured, then after that, all these variables are sampled, then the prediction values of the  $dq$  stator current are computed according to (31) and (32) to utilize them to determine the prediction values of stator flux and the torque in the same time the reference values of the stator flux and torque are calculated through (38). In the last step, the cost function minimizes the errors in the reference and prediction values of the stator and torque according to (35) to apply the voltage, which achieves this minimization.

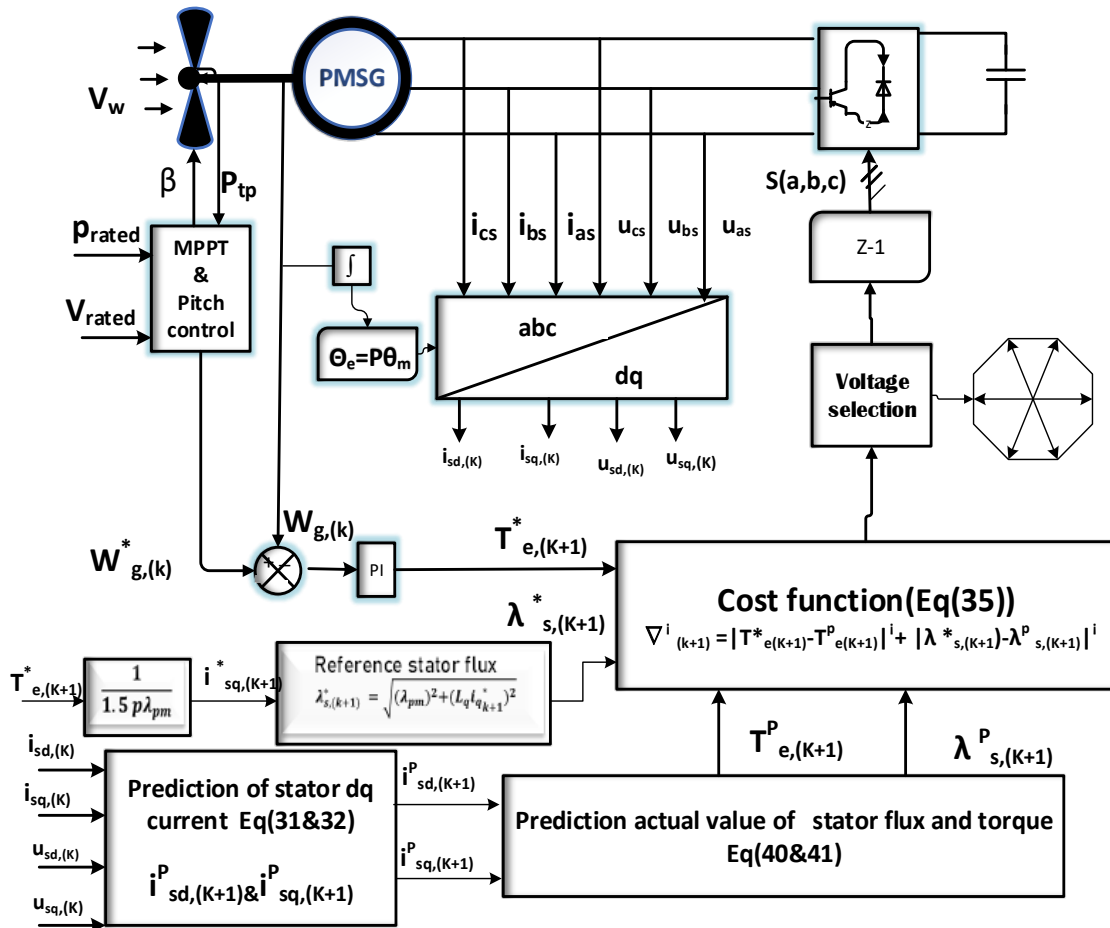


Fig. 10. MPTC for the machine-side converter

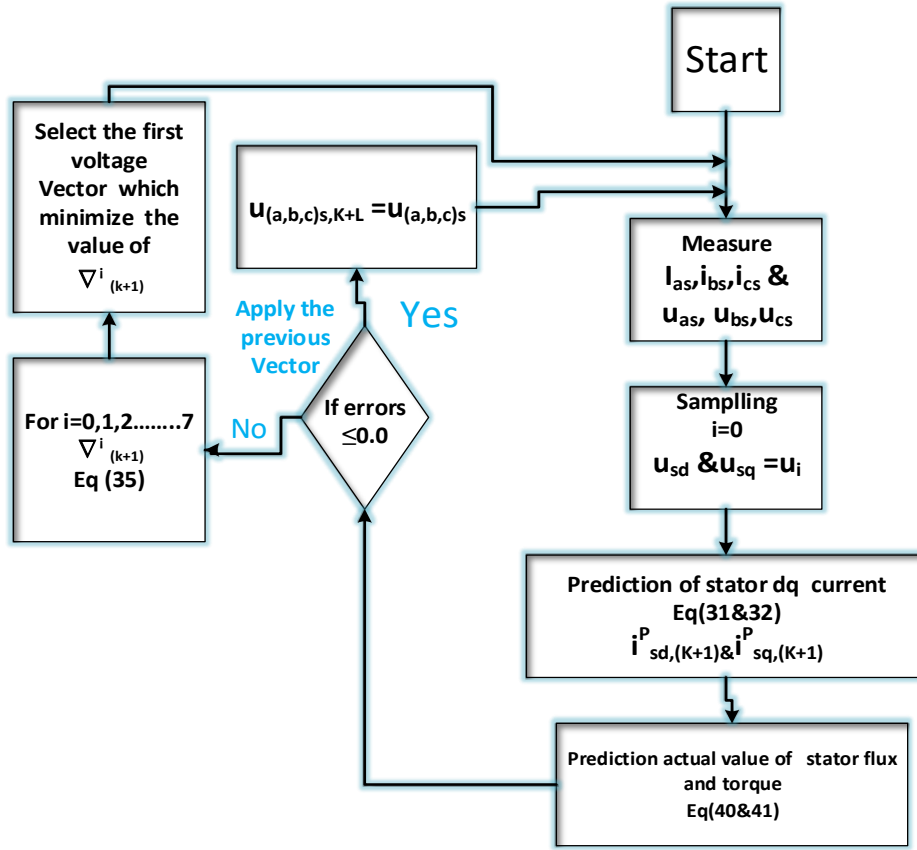


Fig. 11. Flow chart of MPTC for the machine-side converter

### c. The Proposed Predictive Control Approach

The developed PVC utilizes a cost function that combines the absolute errors of the references and predicted quantities of  $d - q$  stator voltage. This cost function has the same units of their variable, so it doesn't require a weighting value. The cost function is expressed as (42).

$$\delta_{k+1}^i = \left| u_{sd,(k+1)}^* - u_{sd,(k+1)}^p \right|^i + \left| u_{sq,(k+1)}^* - u_{sq,(k+1)}^p \right|^i \quad (42)$$

Where  $u_{sd,(k+1)}^*$ ,  $u_{sd,(k+1)}^p$ ,  $u_{sq,(k+1)}^*$ , and  $u_{sq,(k+1)}^p$  are reference stator  $d$  voltage, predictive stator  $d$  voltage, reference  $q$  stator voltage, and predictive stator  $q$  voltage, respectively.

Where  $u_{sd,(k+1)}^p$  and  $u_{sq,(k+1)}^p$  are generated by the switching state of the inverter; while  $u_{sd,(k+1)}^*$ , and  $u_{sq,(k+1)}^*$  are the references of  $d - q$  stator voltage, which are evaluated by using the deadbeat control principle. According to the Deadbeat principle, the reference  $d - q$  stator voltage at the next sampling time is calculated as (43) and (44).

$$u_{sd,(k+1)}^* = R_s L_d i_{sd,(k+1)}^p + L_d \left( \frac{i_{sd,(k+2)}^* - i_{sd,(k+1)}^p}{T_s} \right) - p w_{g,(k+1)} L_q i_{sq,(k+1)}^p \quad (43)$$

$$u_{sq,(k+1)}^* = R_s L_q i_{sq,(k+1)}^p + L_q \left( \frac{i_{sq,(k+2)}^* - i_{sq,(k+1)}^p}{T_s} \right) + p w_{g,(k+1)} L_d i_{sd,(k+1)}^p + P w_{g,(k)} \lambda_{pm} \quad (44)$$

Where the predicted actual values of stator current in  $d - q$  reference frame are obtained by (43). The reference currents in the sample  $(k + 2) Ts$  can be calculated using Lagrange extrapolation as the equation (45) and (46) [57].

$$i_{sd,(k+2)}^* = 3i_{sd,(k)}^* - 3i_{sd,(k-1)}^* + i_{sd,(k-2)}^* \tag{45}$$

$$i_{sq,(k+2)}^* = 3i_{sq,(k)}^* - 3i_{sq,(k-1)}^* + i_{sq,(k-2)}^* \tag{46}$$

Where  $i_{sd,(k)}^*$  is set to zero and  $i_{sq,(k)}^*$  is generated by MPPT, as mentioned earlier. The schematic of the proposed PVC is shown in Fig. 12. The combination of using a deadbeat, which is used to generate the reference of  $d - q$  stator voltage at the next sample time, and a finite control set (FCS), which uses the cost function, in addition to the elimination of the modulator, makes the proposed PVC simpler and faster in its dynamic response, reducing the ripple in the currents, fluxes, and torque in comparison with their values as in MPPT and MPTC, and consequently is considered the most effective approach to be used.

The flow chart is presented in Fig. 13 to display the operation steps of the MPPC. The control begins measuring stator voltage and current and then sample them. After that determines, the prediction values of  $dq$  stator current according to (31), (32) for generating reference values of  $dq$  stator voltages while the predictive value of the stator voltage is generated by the switching state of the inverter. Finally, both the reference and prediction values of the stator voltage are fed to the cost function according to (42).

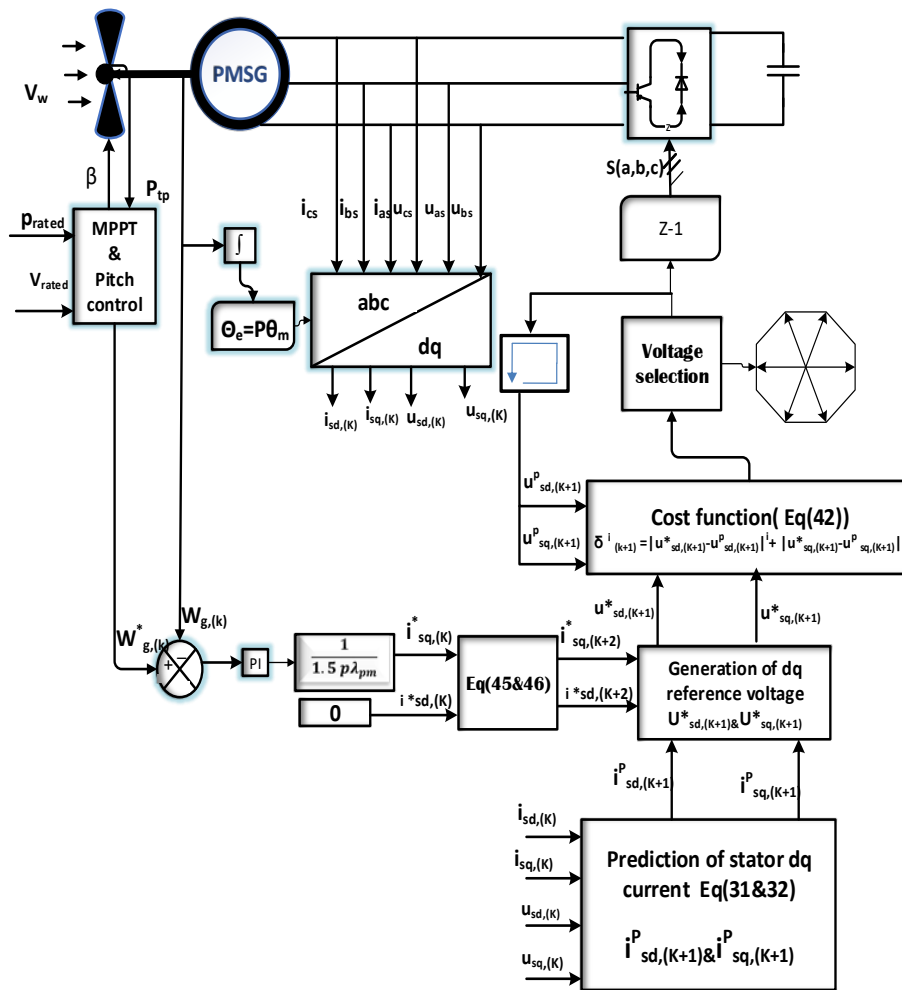


Fig. 12. Proposed PVC for machine-side converter

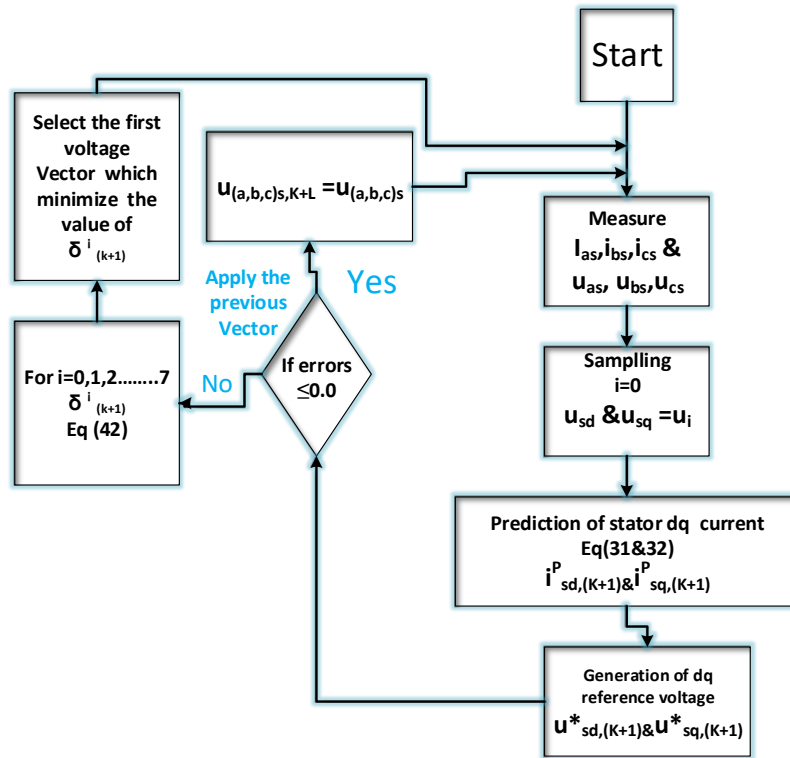


Fig. 13. Flow chart of Proposed PVC for machine-side converter

### 3.3. Abbreviations and Symbols

MPSG	Permanent magnet synchronous generator	$T_m$ & $T_t$ & $T_e$	Mechanical, turbine, and electromagnetic torque
SCIG	Squirrel cage induction generator	$J_{eq}$	Equivalent inertia moment of (the turbine and generator
DFIG	Doubly fed induction generator	$F_r$	Friction of rotor
MPPC	Model predictive power control	$P_{wp}$	Wind power
MPTC	Model predictive Torque control	$P_{tp}$	Turbine power (mechanical power)
PVC	Predictive voltage control	$V_w$	Wind speed
FSC	Finite set control	$A$	Swept area of the wind turbine
TSR	Tip speed ratio	$r$	Radius of blade
FOC	Field oriented control	$P$	Air density
DTC	Direct Torque control	$\lambda_t$	Tip ratio speed
DPC	Direct power control	$T_s$	Time Sampling
SMC	Sliding mode control	$T_{w-g}$	Generator torque
MPPT	Maximum power tracking	$n_g$	Gearbox ratio
$C_p$	Power coefficient	$w_g$	Rotor speed (generator speed)
B	Bitch angle	$U_{gd}$ & $U_{gq}$	$d - q$ voltage at grid side converter
PWM	Pulse width modulation	$I_{gd}$ & $I_{gq}$	$d - q$ grid current
SVPWM	Space vector Pulse width modulation	$V_{gd}$ & $V_{gq}$	$d - q$ grid voltage
SVOC	Stator voltage-oriented control	$R_f$ & $L_f$	Resistance and Inductance of grid filter
MSC	Machine side converter		
GSC	Grid side converter	$P_{gi}$ & $Q_{gi}$	Active and reactive grid power
CF	Cost function	$V_{dc}$ & $I_{dc}$	DC link ed voltage and current
$w_v^p$	The weighting factor for	$P_{s, (k+1)}^*$ & $P_{s, (k+1)}^p$	Reference and predictive stator active

	(MPPC)		power
$w_v^t$	The weighting factor for (MPTC)	$Q_{s,(k+1)}^*$ & $Q_{s,(k+1)}^p$	Reference and predictive stator reactive power
$u_{sd} & u_{sq}$	$d - q$ stator voltage	$i_{sd,(k+1)}^p$ & $i_{sq,(k+1)}^p$	$d - q$ predictive stator current
$i_{sd} & i_{sq}$	$d$ -stator current	$i_{sd,(k+1)}^*$ & $i_{sq,(k+1)}^*$	$d - q$ reference stator current
$\lambda_{sd} & \lambda_{sq}$	$d - q$ stator flux	$u_{sd,(k+1)}^p$ & $u_{sq,(k+1)}^p$	$d - q$ predictive stator voltage
$\lambda_{pm}$	Permanent magnet flux	$u_{sd,(k+1)}^*$ & $u_{sq,(k+1)}^*$	$d - q$ reference stator voltage
$L_d & L_q$	$d - q$ stator inductance	$T_{e,(k+1)}^*$ & $T_{e,(k+1)}^p$	Reference and predictive electromagnetic torque
$W_e & W_g & \omega$	Electrical, Mechanical, and grid angular speed	$\lambda_{s,(k+1)}^*$ & $\lambda_{sq,(k+1)}^p$	Reference and predictive stator flux
$P$	Number of pair poles	$i_{sd,(k+2)}^*$ & $i_{sq,(k+2)}^*$	$d - q$ reference current at $(k + 2)$

#### 4. Results and Discussion

The paper presents the results and discussion of a comparative study of three different controllers for a wind turbine system: MPPC (Model Predictive Power Control), MPTC (Model Predictive Torque Control), and the proposed PVC (Proposed Predictive Voltage Control). The control strategies are evaluated based on various performance metrics such as FFT analysis, commutation burden, the dependence of parameters, and the efficiency compared with each other, whereas the grid-side converter was only controlled by the VOC approach. Fig. 14 depicts the wind speed, which varies from 8m/s to 12m/s at the time ( $t = 5s$ ). Fig. 15 depicts the synchronous generator speed under each of the three control approaches. From Fig. 15, the value of synchronous generator speed for all controllers at the time ( $t = 5s$ ) begins to vary according to the variation in wind speed due to the control dynamics of the wind turbine. There is a link between the applied wind speed and the actual generator speed, and this has been explained in (19), where the turbine speed and the generator speed are equal as a result of using the gearless type. Presenting the proposed PVC control, the fastest dynamic response and the best smooth variation compared with other predictive strategies. Fig. 16 shows the mechanical torque. Fig. 17 depicts the electromagnetic torque for the three controllers, which begins to vary at instant  $t = 5s$  according to the variation of wind speed. The proposed PVC algorithm gives the best dynamic response and the lowest ripple oscillation among all predictive controllers. This is referred to as applying the voltage to the machine directly from the output of the controller without any estimation and prediction as in MPPC and MPTC, so any changes in machine parameters or mistakes don't affect the control making the PVC less ripple and less computation, burden and robustness. Another reason for low ripple and less computation capacity is the eliminating weighting factor from the cost function of the proposed PVC, on the contrary, MPPC and MPTC. Otherwise, the voltage is the first variable that faces the windings making PVC the fastest dynamic response when compared with other predictive controllers, according to the previous figure. Fig. 18 shows the zoomed shot view of electromagnetic torque for three controllers. Fig. 19 depicts the generator's active and reactive powers, which confirm that the proposed PVC has the lowest ripples & fastest dynamic response in comparison to the other predictive control because the const function controls the voltage signal, which is the first variable applied to the machine winding directly from the controller's output rather than the cost function of MPPC needs estimate powers then apply the voltage or estimate torque and flux as in MPTC this makes the proposed PVC faster dynamic response than the other predictive techniques. As a result, any changes in the machine's parameters or errors won't have an impact on the control. This leads to reducing PVC ripple and reducing the commutation load and robustness. The suggested PVC, in contrast to MPPC and MPTC, does not include a weighting element in its cost function, which is another reason for low ripple and reduced computing capacity. Furthermore, Fig.

19 demonstrates the control systems' efficacy in achieving MPPT and pitch angle controls, as the active power follows the wind variation from 8m/s to 12m/s at the same time the reactive power is held constant at zero.

Fig. 20 depicts a zoomed-in view of the power variation to show the detailed power dynamics under various controllers. The  $d - q$  components of the generator stator current, as shown in Fig. 21, vary with wind speed. Besides that, the  $d$ -axis component remains constant and follows the reference value ( $i_{sd,(k+1)}^* = 0$ ) while the  $q$ -axis current follows the variation in wind speed and varies in response to changes in power and mechanical torque. For this reason, we get the shape of  $q$  current similar to the shape of torque and power. Fig. 22 shows a zoomed-in view of the  $d - q$  current components to show the deviation from the reference currents under the three different control systems. It is vividly that the PVC method guarantees the lowest average oscillation and more robustness and stability in this figure as the result of eliminating the weighting factor from its cost function and applying the voltage, which doesn't require any estimation from machine parameters on the contrary of MPPC and MPTC as mentioned before. Fig. 23 to Fig. 25 depict the three-phase stator currents under MPPC, MPTC, and suggested PVC control. Based on these figures, it can be demonstrated that the designed PVC strategy has the lowest current harmonics, which is referred to the effects of applying voltage without dependence on machine parameters so the oscillation of voltage becomes low. Consequently, the current becomes less harmonic distortion as we get the current from the voltage, so power becomes the highest quality and the fastest dynamic response when compared to machine-side controllers, thereby validating the PVC's effectiveness. This was also explored using FFT analysis for the stator-generated currents, as will be shown later. The grid current's  $d - q$  components are displayed in Fig. 26. Remarkably, the  $d$ -axis grid current is held at zero tracking the reactive power for maintaining the power factor at the unity value. On the contrary side, the change in active power is tracked by  $d$  axis grid current. Fig. 27 gives an in-depth look at the  $dq$  grid current components which  $q$  grid current follows the reference  $I_{gq}^* = 0$  to achieve a unity power factor and proved that PVC has smooth dynamics response and low current oscillation referring to the effect of applying the voltage and eliminating the weighting factor from its cost function. Last but not least, Fig. 28 displays the DC link voltage for all controllers where the PVC keeps the voltage at its reference with the fewest oscillations and the fastest dynamic response in comparison to the other predictive algorithms. The reason behind this is the dc link voltage changes; with wind variation to be held at constant value must, the power input from the generator equals the out power to avoid the dc voltage varying with reference speed. Surely the stator power under the proposed PVC is low ripple as a result of the dc link voltage of PVC having the lowest ripple than the others.

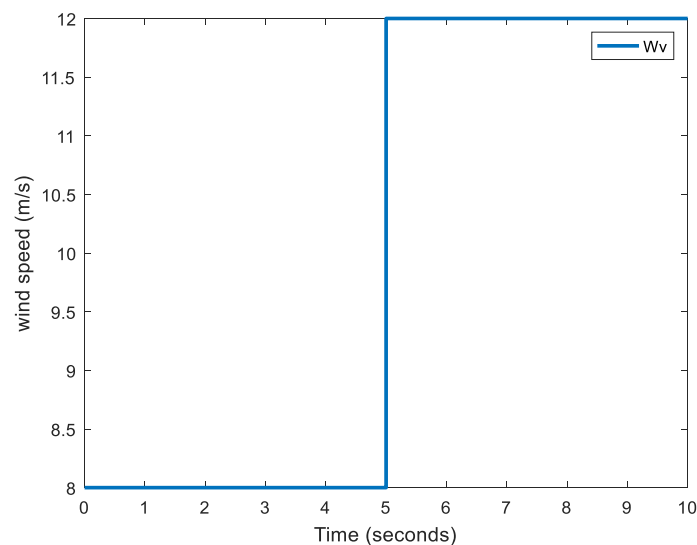


Fig. 14. Wind speed changes from 8m/s to 12m/s

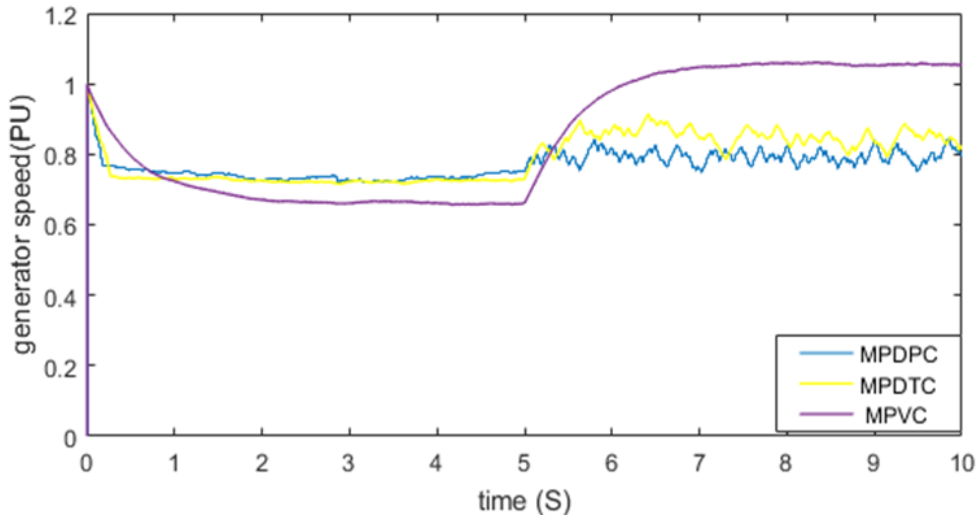


Fig. 15. Generator speed

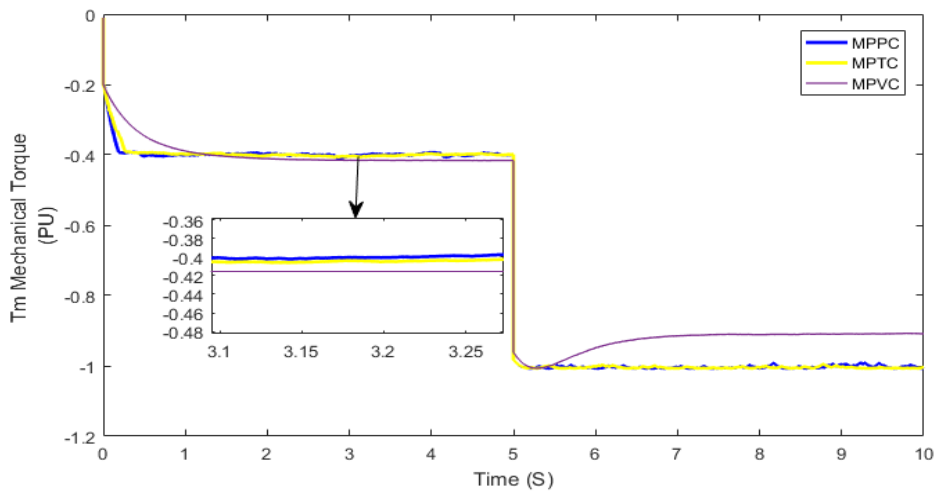


Fig. 16. Mechanical torque

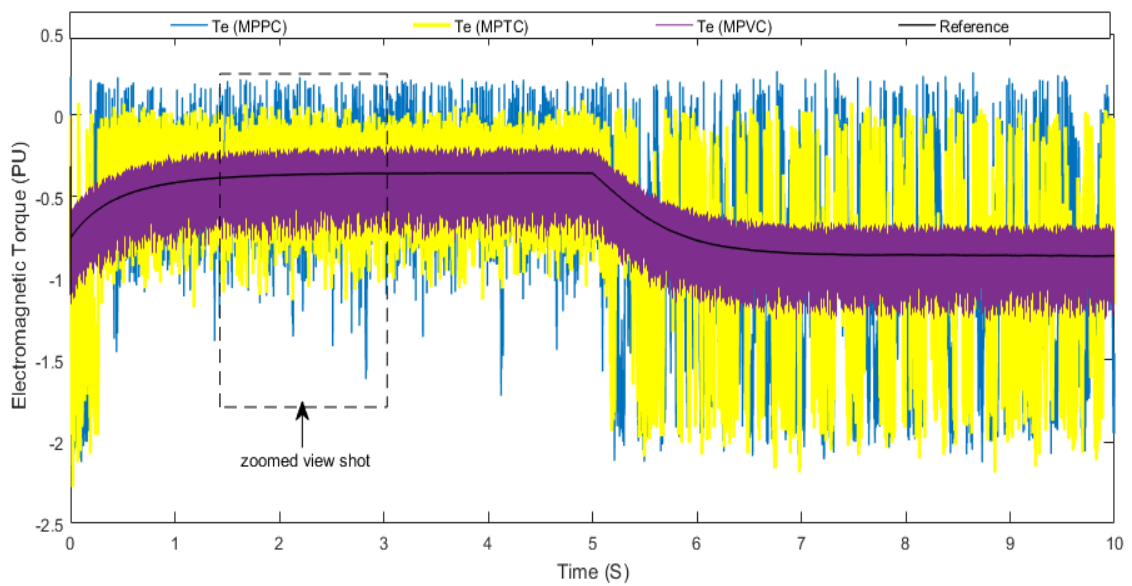


Fig. 17. Electromagnetic torque

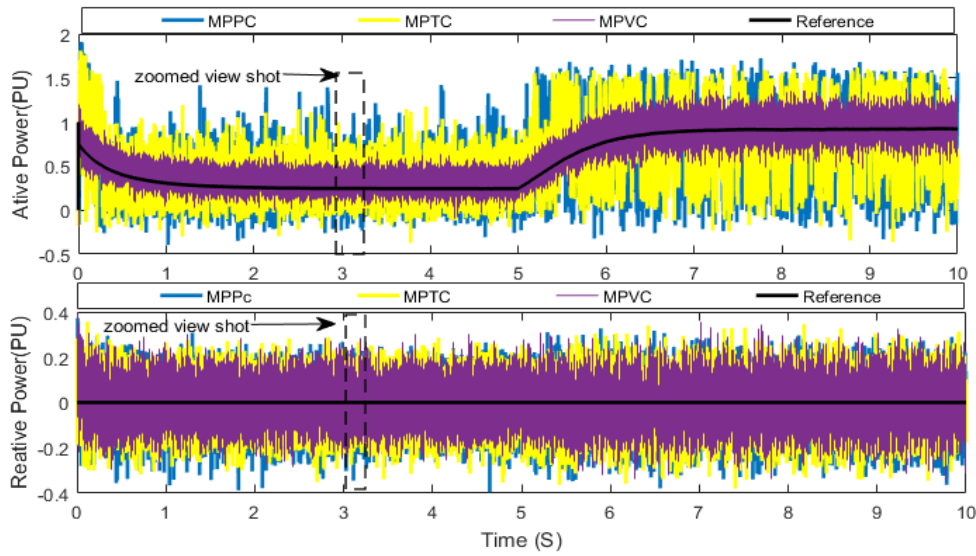


Fig. 18. Zoomed view shot of electromagnetic torque

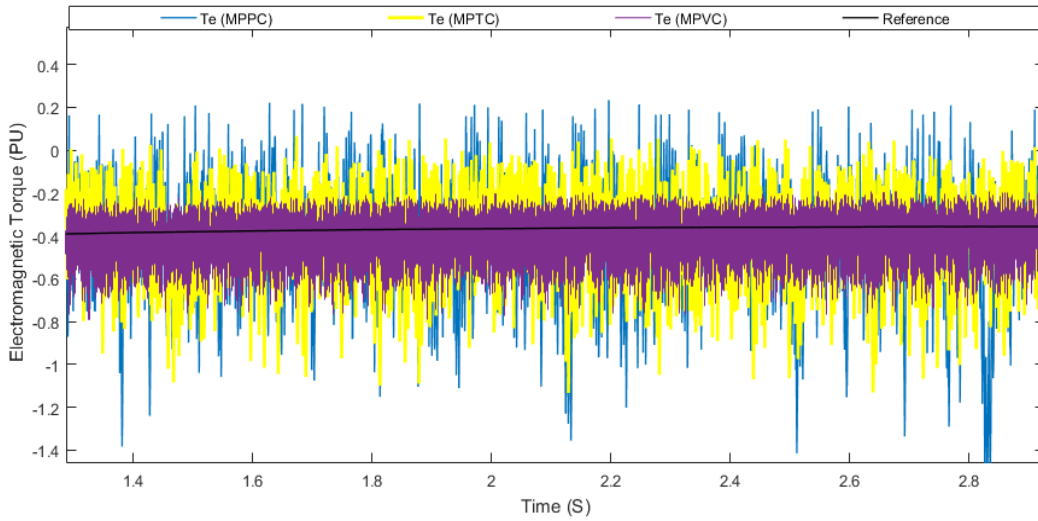


Fig. 19. Generated active and reactive power

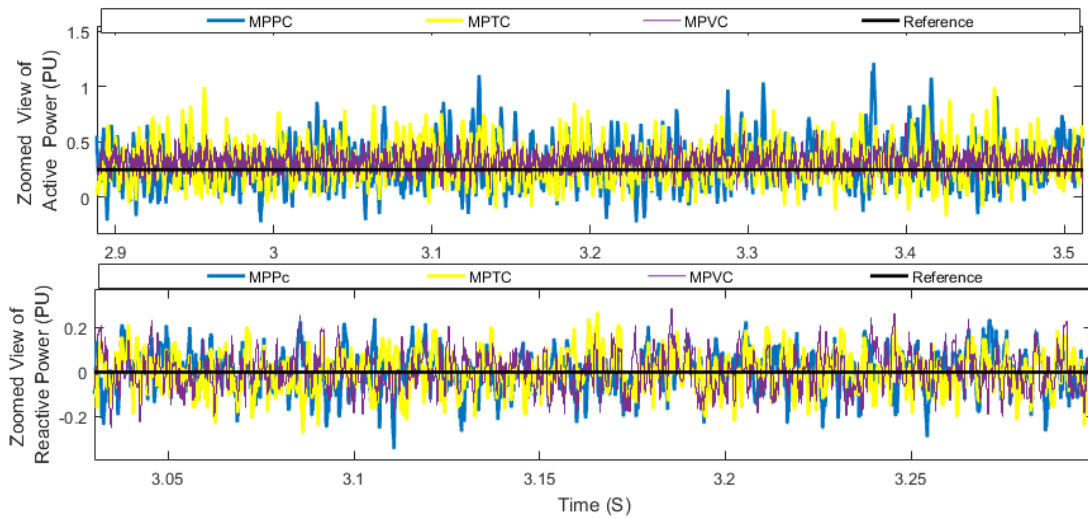
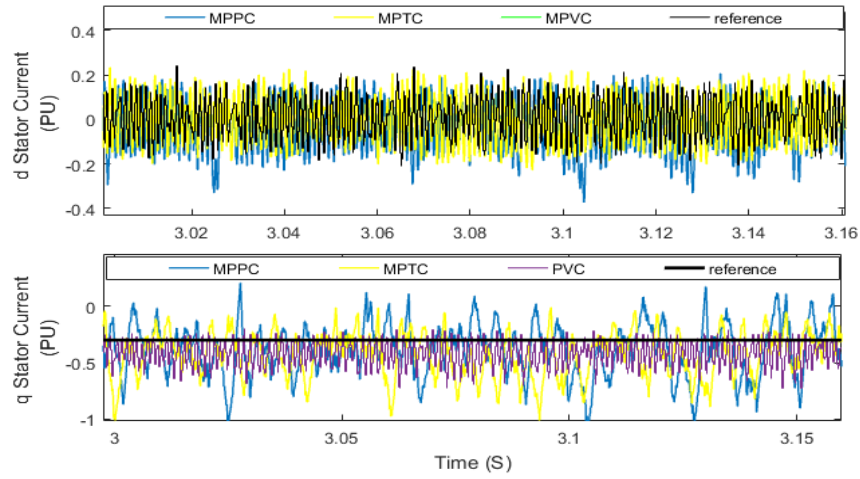
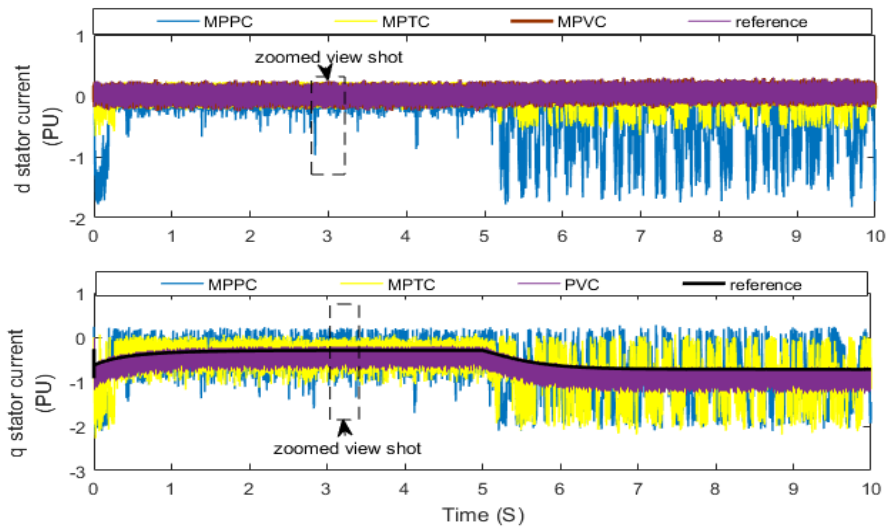


Fig. 20. Zoomed view of generated active and reactive power



**Fig. 21.**  $d - q$  stator currents



**Fig. 22.** Zoomed view of  $d - q$  stator currents

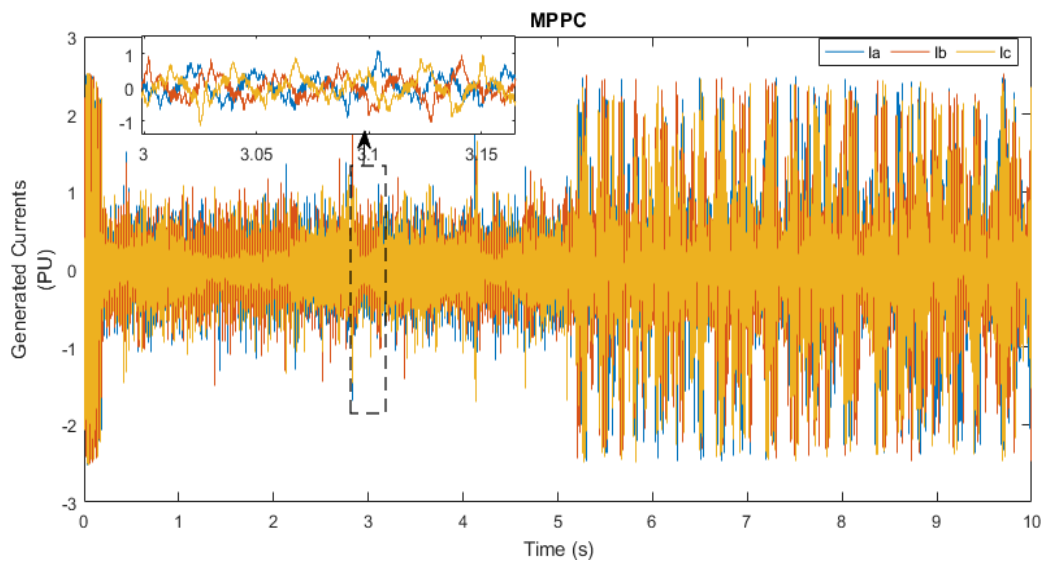


**Fig. 23.** Three-phase stator current of MPPC

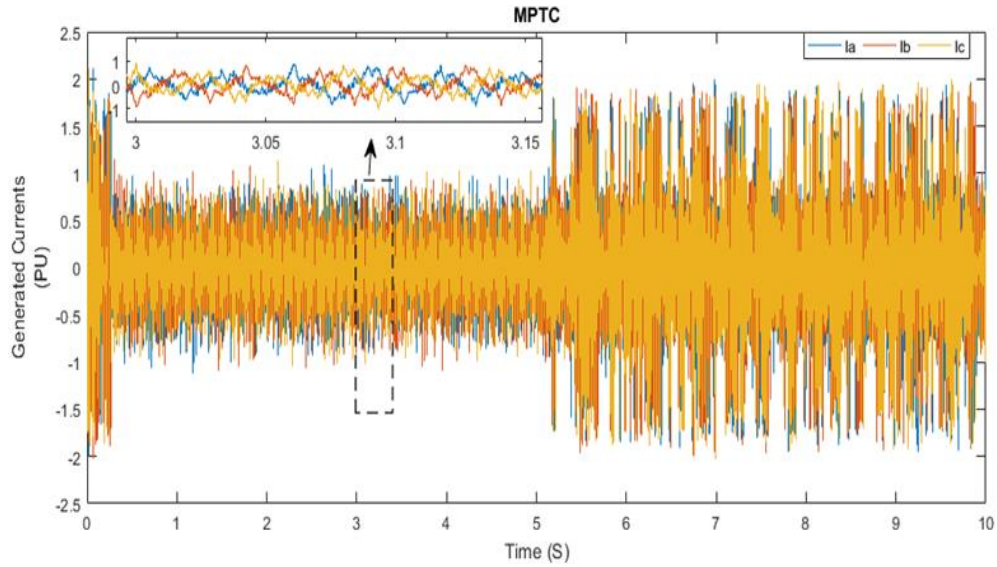


Fig. 24. Three-phase stator current of MPTC

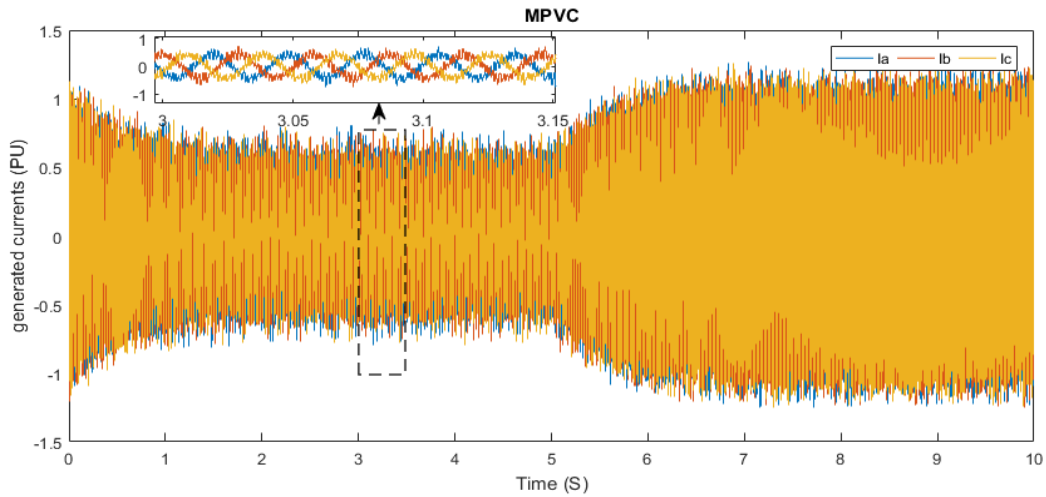


Fig. 25. Three-phase stator current of the model proposed PVC.

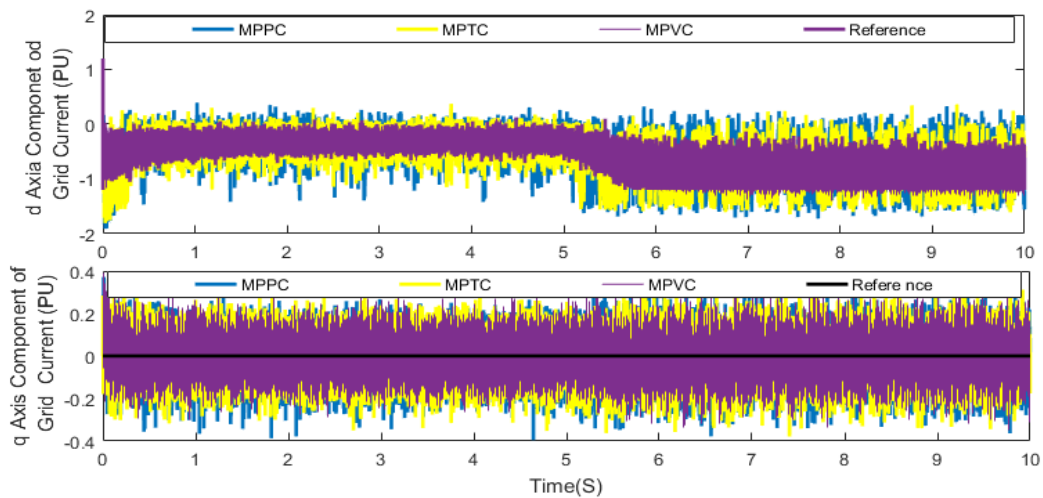


Fig. 26.  $d - q$  grid currents

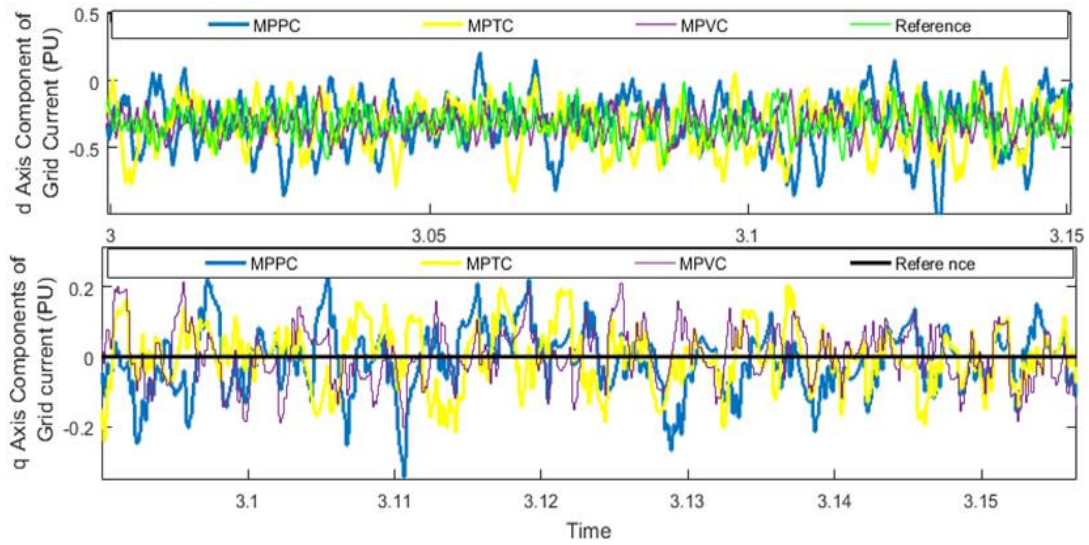


Fig. 27. Zoomed view shot of  $d - q$  grid currents

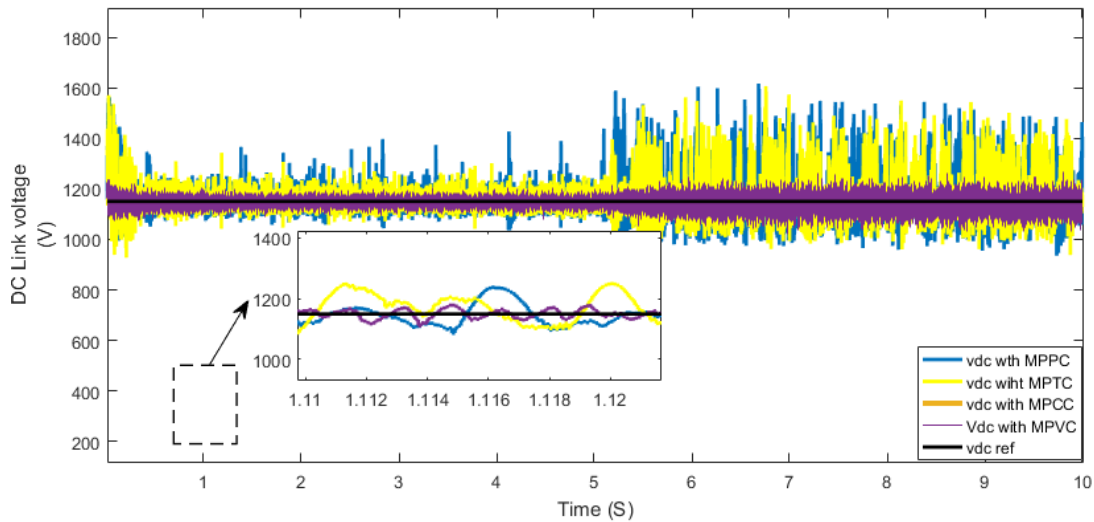


Fig. 28. DC link voltage

Table 1 displays the outcomes for all three control systems in terms of the number of commutations. This variable is taken into account as an indicator of the amount of computational help each controller can offer. To satisfy the requirements of microcontrollers that manage the control process, it is strongly suggested to maintain a minimal burden. The results in the table demonstrate that the PVC has the fewest commutations and efficiently assists in decreasing the computation burden, which helps in limiting switching losses, which is regarded as one of the greatest problems of predictive control strategies. Surely the reasons behind low commutations are the eliminating weight factor from its cost function and applying the voltage without needing any estimation, as mentioned earlier.

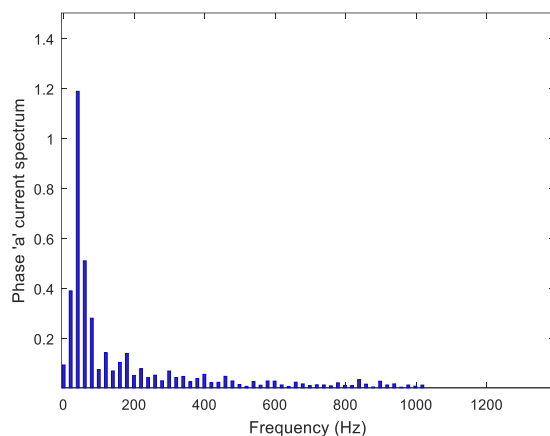
Table 1. Three model predictive controllers' commutation numbers

Control Strategy	Commutation number for MSC Controllers	
	Commutation's number	
MPPC	5641	
MPTC	6150	
Proposed PVC	4770	

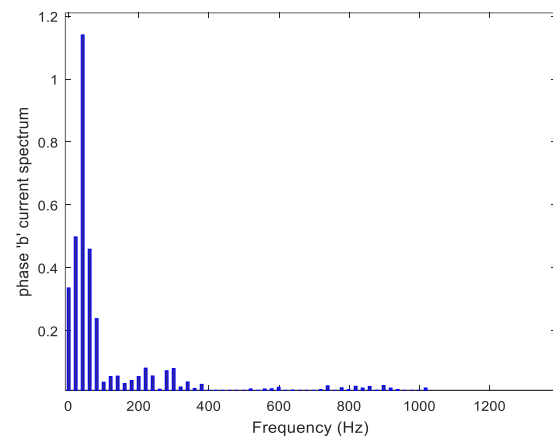
The FFT spectrum analysis for the stator currents is presented in graphical forms for the three predictive controllers sequentially from Fig. 29 to Fig. 31 and in numerical form in Table 2. The statistics confirm the effectiveness of the proposed PVC in achieving lower THD in generated current signals in comparison with the other predictive techniques. The reason behind this result is the mechanism cost function of Propped PVC depends on controlling variables ( $dq$  stator voltages) and doesn't depend on machine parameters leading to applying a reference voltage with low oscillation and generating current with low harmonics. On the contrary, the cost function MPPC generates reference voltage indirectly by managing the active and reactive power, which depends on machine parameters or MPTC's cost function, which manages the flux and torque. Another reason is the elimination weighting factor which chooses an inaccurate value causing increasing the ripple and number of commutations, as mentioned earlier. All of these helped effectively in ensuring high power quality using the proposed PVC.

**Table 2.** FFT analysis of stator currents for the three predictive controllers with MSC

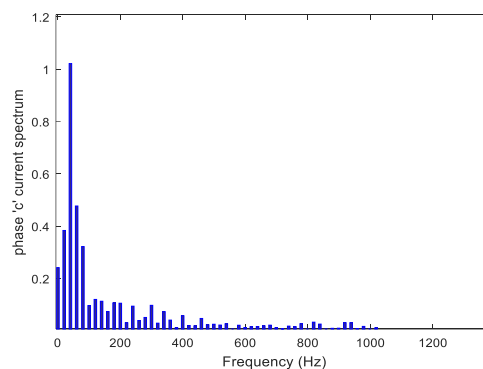
Type of Control	THD of Phases Current		
	Phase a	Phase b	Phase c
MPPC	Fundamental: 0.510795 THD = 54.69 %	Fundamental: 0.45899 THD = 33.71 %	Fundamental: 0.47718 THD = 56.11 %
MPTC	Fundamental: 0.342677 THD = 48.28 %	Fundamental: 0.256227 THD = 44.84 %	Fundamental: 0.423012 THD = 39.01 %
Proposed PVC	Fundamental: 0.740161 THD = 15.16 %	Fundamental: 0.783106 THD = 21.31 %	Fundamental: 0.827769 THD = 24.39 %



(a) Spectrum analysis of phase a

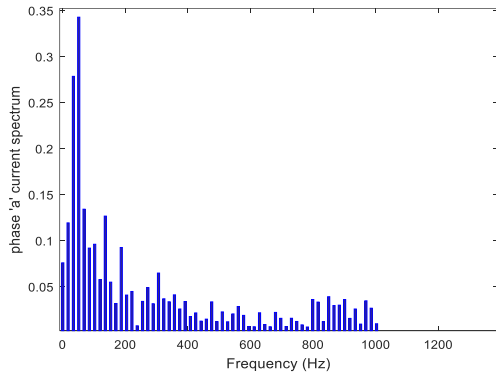


(b) Spectrum analysis of phase b

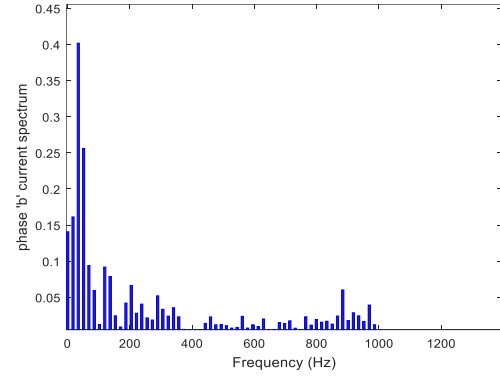


(c) Spectrum analysis of phase c

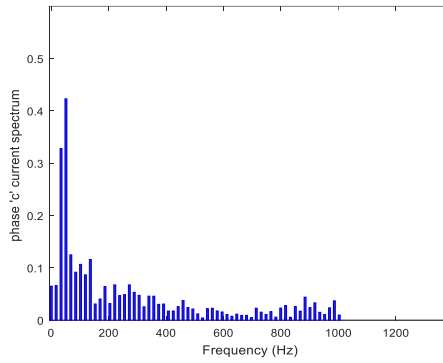
**Fig. 29.** Current spectrum analysis for stator currents under MPPC



(a) Spectrum analysis of phase a

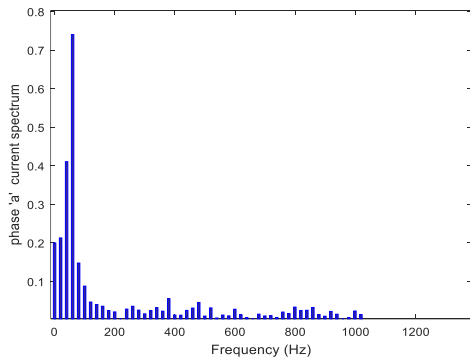


(b) Spectrum analysis of phase b

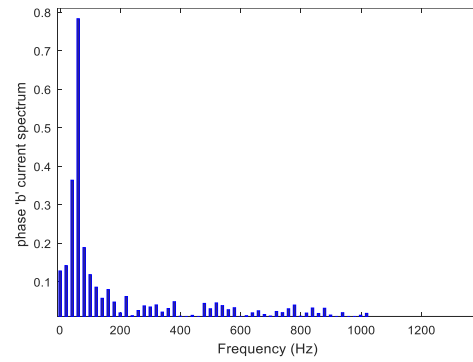


(c) Spectrum analysis of phase c

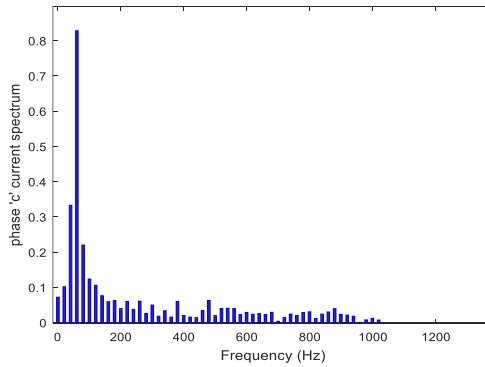
**Fig. 30.** Current spectrum analysis for stator currents under MPTC



(a) Spectrum analysis of phase a



(b) Spectrum analysis of phase b



(c) Spectrum analysis of phase c

**Fig. 31.** Current spectrum analysis for stator currents under proposed PVC

## 5. Conclusion

The paper adopted three various control methods to offer a thorough dynamic performance analysis of a variable speed wind-driven PMSG. These analyses are discussed which controls give the fastest dynamic response, lowest ripple, lowest computation capacity, and independence of machine parameters. The considered controllers are the model predictive power (MPPC), model predictive torque (MPTC), and proposed predictive voltage (PVC) control schemes. In contrast to the traditional predictive controllers, the proposed PVC approach has a simpler concept because of using a simple cost function, not needing any PI regulator, and using the FCS principle for selecting the optimum voltages, which led to eliminating to use of PWM, low ripple and low commutation as the result of its cost function doesn't need any weighting factor and the variables (the components of the voltages) used in this cost function don't need any estimation leading to robustness against parameters variation and ensuring high quality of power due to reducing the ripple in addition to the reducing torque ripple which is a vital requirement to reduce the shaft variation and prevent the mechanical problem and also The fast response of the proposed control is an important need to deal with the variation of the wind. The wind turbine control system is formulated with maximum power point tracking and pitch angle control, which are very important control to extract the maximum power in case the generator speed is under its rated speed by maintaining the cubic relationship between the wind and power and limit wind energy utilization in case of strong wind by increasing the pitch angle so power coefficient decreased. In addition, a detailed comparison was presented between all machine-side controllers in terms of construct and THD currents. The outcomes represent that the proposed PVC controller had the most effective dynamic performance and lowest computation burdens in comparison with the other controllers, confirmed by its simple structure, low ripples, and low current harmonics, more efficiency and robustness against the variation leading to the achievement of the reliability of the system. In general, the designed predictive control can be used with another generator type, like a double field induction generator and multiphase generator or turbine wind, after considering the structure of each generator and turbine.

**Author Contribution:** All authors contributed equally to the main contributor to this paper. All authors read and approved the final paper.

**Funding:** This research received no external funding.

**Conflicts of Interest:** The authors declare no conflict of interest.

## Appendix

**Table 1A.** Data specifications for PMSG and turbine

Parameters	Value
$R_s$	0.006 $\Omega$
$L_d = L_q = L_s$	0.5131H
Linkage flux ( $\lambda_{pm}$ )	1.48Wb
Inertia	35000kg.m <sup>2</sup>
viscous damping	0.01 Nms
pole pairs	48
Rated apparent power	1.5e6VA
Rated power	1.35MW
DC capacitor voltage	1150V
Rated L-L voltage	575V
Sampling time	0.0001s
Rated Frequency	50Hz
Specific air density ( $\rho$ )	1.12kg/m <sup>3</sup>
Turbine rotor radius	33.05m
Rated wind speed	12m/s

**Table 2A.** Parameters of current controllers for grid-side converter

Parameter	Value
$K_p$	0.83
$K_i$	5

## References

- [1] X. Xie, Y. Zhang, K. Meng, Z. Y. Dong, and J. Liu, "Emergency control strategy for power systems with renewables considering a utility-scale energy storage transient," in *CSEE Journal of Power and Energy Systems*, vol. 7, no. 5, pp. 986-995, Sept. 2021, <https://doi.org/10.17775/CSEEJPES.2019.02320>.
- [2] M. Nurunnabi, N. K. Roy, E. Hossain, and H. R. Pota, "Size Optimization and Sensitivity Analysis of Hybrid Wind/PV Micro-Grids- A Case Study for Bangladesh," in *IEEE Access*, vol. 7, pp. 150120-150140, 2019, <https://doi.org/10.1109/ACCESS.2019.2945937>.
- [3] P. Sadorsky, "Wind energy for sustainable development: Driving factors and future outlook," *J. Clean. Prod.*, vol. 289, p. 125779, 2021, <https://doi.org/10.1016/j.jclepro.2020.125779>.
- [4] D. Kotin, I. Ivanov, and S. Shtukkert, "Modified Permanent Magnet Synchronous Generators for Using in Energy Supply System for Autonomous Consumer," *Energies*, vol. 14, no. 21, p. 7196, Nov. 2021, <https://doi.org/10.3390/en14217196>.
- [5] R. Banos, F. M. Agugliaro, F. G. Montoya, C. Gil, A. Alcayde, and J. Gómez, "Optimization methods applied to renewable and sustainable energy: A review," *Renewable and sustainable energy reviews*, vol. 15, no. 4, pp. 1753-1766, 2011, <https://doi.org/10.1016/j.rser.2010.12.008>.
- [6] U. K. Pata, "Renewable and non-renewable energy consumption, economic complexity, CO2 emissions, and ecological footprint in the USA: testing the EKC hypothesis with a structural break," *Environ. Sci. Pollut. Res.*, vol. 28, no. 1, pp. 846-861, 2021, <https://doi.org/10.1007/s11356-020-10446-3>.
- [7] W. Dong, G. Zhao, S. Yüksel, H. Dinçer, and G. G. Ubay, "A novel hybrid decision making approach for the strategic selection of wind energy projects," *Renew. Energy*, vol. 185, pp. 321-337, Feb. 2022, <https://doi.org/10.1016/j.renene.2021.12.077>.
- [8] M. A. Husain and A. Tariq, "Modeling and Study of a Standalone PMSG Wind Generation System Using MATLAB/SIMULINK" *Univers. J. Electr. Electron. Eng.*, vol. 2, no. 7, pp. 270-277, 2014, <https://doi.org/10.13189/ujjee.2014.020702>.
- [9] O. J. Tola, E. A. Umoh, E. A. Yahaya, and O. E. Olusegun, "Permanent Magnet Synchronous Generator Connected to a Grid via a High Speed Sliding Mode Control," *International Journal of Robotics & Control Systems*, vol. 2, no. 2, pp. 379-395, 2022, <https://doi.org/10.31763/ijrcs.v2i2.701>.
- [10] V. Yaramasu and B. Wu. *Model predictive control of wind energy conversion systems*. John Wiley & Sons, 2016, <https://books.google.co.id/books?id=PTlxDQAAQBAJ>.
- [11] S. W. Lee and K. H. Chun, "Adaptive sliding mode control for PMSG wind turbine systems," *Energies*, vol. 12, no. 4, 2019, <https://doi.org/10.3390/en12040595>.
- [12] W. Yang and J. Yang, "Advantage of variable-speed pumped storage plants for mitigating wind power variations: Integrated modelling and performance assessment," *Appl. Energy*, vol. 237, pp. 720-732, 2019, <https://doi.org/10.1016/j.apenergy.2018.12.090>.
- [13] Z. Zhang, Y. Zhao, W. Qiao, and L. Qu, "A Discrete-Time Direct Torque Control for Direct-Drive PMSG-Based Wind Energy Conversion Systems," in *IEEE Transactions on Industry Applications*, vol. 51, no. 4, pp. 3504-3514, July-Aug. 2015, <https://doi.org/10.1109/TIA.2015.2413760>.
- [14] A. Luna, P. Rodriguez, R. Teodorescu, and F. Blaabjerg, "Low voltage ride through strategies for SCIG wind turbines in distributed power generation systems," *2008 IEEE Power Electronics Specialists Conference*, pp. 2333-2339, 2008, <https://doi.org/10.1109/PESC.2008.4592290>.
- [15] M. A. Mossa, T. D. Do, A. S. Al-Sumaiti, N. V. Quynh, and A. A. Z. Diab, "Effective Model Predictive Voltage Control for a Sensorless Doubly Fed Induction Generator," in *IEEE Canadian Journal of*

- Electrical and Computer Engineering*, vol. 44, no. 1, pp. 50-64, 2021, <https://doi.org/10.1109/ICJECE.2020.3018495>.
- [16] M. Mossa and Y. Mohamed, "Novel scheme for improving the performance of a wind driven doubly fed induction generator during grid fault," *Wind Engineering*, vol. 36, no. 3, pp. 305–334, 2012, <https://doi.org/10.1260/0309-524X.36.3.305>.
- [17] M. A. Mossa, A. Saad Al-Sumaiti, T. Duc Do, and A. A. Zaki Diab, "Cost-Effective Predictive Flux Control for a Sensorless Doubly Fed Induction Generator," in *IEEE Access*, vol. 7, pp. 172606-172627, 2019, <https://doi.org/10.1109/ACCESS.2019.2951361>.
- [18] M. E. Moore, "Making connections," *Relig. Educ.*, vol. 78, no. 4, pp. 510–515, 1983, <https://doi.org/10.1080/0034408300780412>.
- [19] M. A. Mossa, O. Gam, N. Bianchi, and N. V. Quynh, "Enhanced Control and Power Management for a Renewable Energy-Based Water Pumping System," in *IEEE Access*, vol. 10, pp. 36028-36056, 2022, <https://doi.org/10.1109/ACCESS.2022.3163530>.
- [20] L. Pan and C. Shao, "Wind energy conversion systems analysis of PMSG on offshore wind turbine using improved SMC and Extended State Observer," *Renew. Energy*, vol. 161, pp. 149–161, 2020, <https://doi.org/10.1016/j.renene.2020.06.057>.
- [21] E. C. Navarrete, M. T. Perea, J. C. J. Correa, R. V. C. Serrano, and G. J. R. Moreno, "Expert Control Systems Implemented in a Pitch Control of Wind Turbine: A Review," in *IEEE Access*, vol. 7, pp. 13241-13259, 2019, <https://doi.org/10.1109/ACCESS.2019.2892728>.
- [22] K. Palanimuthu, G. Mayilsamy, S. R. Lee, S. Y. Jung, and Y. H. Joo, "Comparative analysis of maximum power extraction and control methods between PMSG and PMVG-based wind turbine systems," *Int. J. Electr. Power Energy Syst.*, vol. 143, p. 108475, Dec. 2022, <https://doi.org/10.1016/j.ijepes.2022.108475>.
- [23] S. Qin, Y. Chang, Z. Xie, and S. Li, "Improved Virtual Inertia of PMSG-Based Wind Turbines Based on Multi-Objective Model-Predictive Control," *Energies*, vol. 14, no. 12, p. 3612, 2021, <https://doi.org/10.3390/en14123612>.
- [24] Z. Wang, J. Chen, M. Cheng, and K. T. Chau, "Field-Oriented Control and Direct Torque Control for Paralleled VSIs Fed PMSM Drives With Variable Switching Frequencies," in *IEEE Transactions on Power Electronics*, vol. 31, no. 3, pp. 2417-2428, March 2016, <https://doi.org/10.1109/TPEL.2015.2437893>.
- [25] M. A. Mossa, O. M. Kamel, and S. Bolognani, "Explicit Predictive Voltage Control for an Induction Motor Drive," *2019 21st International Middle East Power Systems Conference (MEPCON)*, pp. 258-264, 2019, <https://doi.org/10.1109/MEPCON47431.2019.9008029>.
- [26] Y. Sahri *et al.*, "Effectiveness analysis of twelve sectors of DTC based on a newly modified switching table implemented on a wind turbine DFIG system under variable wind velocity," *Ain Shams Engineering Journal*, p. 102221, 2023, <https://doi.org/10.1016/j.asej.2023.102221>.
- [27] A. Harrouz, A. Benatiallah, and O. Harrouz, "Direct power control of a PMSG dedicated to standalone wind energy systems," *2013 Eighth International Conference and Exhibition on Ecological Vehicles and Renewable Energies (EVER)*, pp. 1-5, 2013, <https://doi.org/10.1109/EVER.2013.6521556>.
- [28] A. Izanlo, S. A. Gholamian, and M. V. Kazemi, "Comparative study between two sensorless methods for direct power control of doubly fed induction generator," *Revue Roumaine des Sciences Techniques Serie Electrotechnique et Energetique*, vol. 62, no. 4, pp. 358–364, 2017, <http://revue.elth.pub.ro/index.php?action=details&id=703>.
- [29] M. A. Mossa and S. Bolognani, "Effective model predictive direct torque control for an induction motor drive," *2016 International Symposium on Power Electronics, Electrical Drives, Automation and Motion (SPEEDAM)*, pp. 746-754, 2016, <https://doi.org/10.1109/SPEEDAM.2016.7525814>.
- [30] Z. Zhang, Z. Cui, Z. Zhang, R. Kennel, and J. Rodríguez, "Advanced Control Strategies for Back-to-Back Power Converter PMSG Wind Turbine Systems," *2019 IEEE International Symposium on Predictive Control of Electrical Drives and Power Electronics (PRECEDE)*, pp. 1-6, 2019, <https://doi.org/10.1109/PRECEDE.2019.8753366>.

- 
- [31] M. Alsumiri and R. Althomali, "Enhanced Low Voltage Ride through Capability for Grid Connected Wind Energy Conversion System," *Int. J. Robot. Control Syst.*, vol. 1, no. 3, pp. 369–377, 2021, <https://doi.org/10.31763/ijrcs.v1i3.441>.
- [32] M. A. Mossa, H. Echeikh, N. El Ouanjli, and H. H. Alhelou, "Enhanced Second-Order Sliding Mode Control Technique for a Five-Phase Induction Motor," *Int. Trans. Electr. Energy Syst.*, vol. 2022, 2022, <https://doi.org/10.1155/2022/8215525>.
- [33] A. A. Z. Diab, A. A. Ahmed, and H. A. Abdelsalam, "Fuzzy-based Adaptive Sliding Mode Control for a Direct-Driven PMSG Wind Energy System," *2019 21st International Middle East Power Systems Conference (MEPCON)*, pp. 81-88, 2019, <https://doi.org/10.1109/MEPCON47431.2019.9008013>.
- [34] S. M. Mozayan, M. Saad, H. Vahedi, H. Fortin-Blanchette, and M. Soltani, "Sliding Mode Control of PMSG Wind Turbine Based on Enhanced Exponential Reaching Law," in *IEEE Transactions on Industrial Electronics*, vol. 63, no. 10, pp. 6148-6159, Oct. 2016, <https://doi.org/10.1109/TIE.2016.2570718>.
- [35] M. R. M. Hassan, M. A. Mossa, and G. M. Dousoky, "Evaluation of electric dynamic performance of an electric vehicle system using different control techniques," *Electronics*, vol. 10, no. 21, pp. 1–34, 2021, <https://doi.org/10.3390/electronics10212586>.
- [36] A. A. Ahmed, A. Bakeer, H. H. Alhelou, P. Siano, and M. A. Mossa, "A new modulated finite control set-model predictive control of quasi-Z-source inverter for PMSM drives," *Electronics*, vol. 10, no. 22, 2021, <https://doi.org/10.3390/electronics10222814>.
- [37] M. A. Mossa, M. K. Abdelhamid, A. A. Hassan, and N. Bianchi, "Improving the Dynamic Performance of a Variable Speed DFIG for Energy Conversion Purposes Using an Effective Control System," *Processes*, vol. 10, no. 3, p. 456, 2022, <https://doi.org/10.3390/pr10030456>.
- [38] Z. Zhang, H. Fang, F. Gao, J. Rodríguez, and R. Kennel, "Multiple-Vector Model Predictive Power Control for Grid-Tied Wind Turbine System With Enhanced Steady-State Control Performance," in *IEEE Transactions on Industrial Electronics*, vol. 64, no. 8, pp. 6287-6298, Aug. 2017, <https://doi.org/10.1109/TIE.2017.2682000>.
- [39] M. A. Mossa and S. Bolognani, "Predictive Power Control for a Linearized Doubly Fed Induction Generator Model," *2019 21st International Middle East Power Systems Conference (MEPCON)*, pp. 250-257, 2019, <https://doi.org/10.1109/MEPCON47431.2019.9008085>.
- [40] M. A. Mossa, O. Gam, and N. Bianchi, "Dynamic Performance Enhancement of a Renewable Energy System for Grid Connection and Stand-Alone Operation with Battery Storage," *Energies*, vol. 15, no. 3, p. 1002, 2022, <https://doi.org/10.3390/en15031002>.
- [41] L. Guo, X. Zhang, S. Yang, Z. Xie, L. Wang, and R. Cao, "Simplified model predictive direct torque control method without weighting factors for permanent magnet synchronous generator-based wind power system," *IET Electric Power Applications*, vol. 11, no. 5, pp. 793-804, 2017, <https://doi.org/10.1049/iet-epa.2015.0620>.
- [42] G. Zhang, C. Chen, X. Gu, Z. Wang, and X. Li, "An improved model predictive torque control for a two-level inverter fed interior permanent magnet synchronous motor," *Electronics*, vol. 8, no. 7, 2019, <https://doi.org/10.3390/electronics8070769>.
- [43] M. A. Mossa, N. E. Ouanjli, O. Gam, and O. M. Kamel, "Performance improvement of a hybrid energy system feeding an isolated load," *2022 23rd International Middle East Power Systems Conference (MEPCON)*, pp. 1-8, 2022, <https://doi.org/10.1109/MEPCON55441.2022.10021715>.
- [44] M. A. Mossa and S. Bolognani, "Effective model predictive current control for a sensorless IM drive," *2017 IEEE International Symposium on Sensorless Control for Electrical Drives (SLED)*, pp. 37-42, 2017, <https://doi.org/10.1109/SLED.2017.8078427>.
- [45] H. Echeikh, N. V. Quynh, H. H. Alhelou, A. A. Ahmed, and M. A. Mossa, "Enhancement of induction motor dynamics using a novel sensorless predictive control algorithm," *Energies*, vol. 14, no. 14, 2021, <https://doi.org/10.3390/en14154401>.
-

- [46] P. Gajewski and K. Pieńkowski, "Bezpośrednie sterowanie momentem i mocą w systemie elektrowni wiatrowej z generatorem PMSG," *Przegląd Elektrotechniczny*, vol. 92, no. 10, pp. 249–253, 2016, <https://doi.org/10.15199/48.2016.10.56>.
- [47] L. Shengquan, L. Juan, T. Yongwei, S. Yanqiu, and C. Wei, "Model-based model predictive control for a direct-driven permanent magnet synchronous generator with internal and external disturbances," *Trans. Inst. Meas. Control*, vol. 42, no. 3, pp. 586–597, 2020, <https://doi.org/10.1177/0142331219878574>.
- [48] G. Mayilsamy *et al.*, "A Review of State Estimation Techniques for Grid-Connected PMSG-Based Wind Turbine Systems," *Energies*, vol. 16, no. 2, pp. 1–27, 2023, <https://doi.org/10.3390/en16020634>.
- [49] O. Alizadeh and A. Yazdani, "A Strategy for Real Power Control in a Direct-Drive PMSG-Based Wind Energy Conversion System," in *IEEE Transactions on Power Delivery*, vol. 28, no. 3, pp. 1297–1305, July 2013, <https://doi.org/10.1109/TPWRD.2013.2258177>.
- [50] M. A. Mossa, O. Gam, and N. Bianchi, "Performance Enhancement of a Hybrid Renewable Energy System Accompanied with Energy Storage Unit Using Effective Control System," *International Journal of Robotics and Control Systems*, vol. 2, no. 1, pp. 140–171, 2022, <https://doi.org/10.31763/ijrcs.v2i1.599>.
- [51] M. E. Emna, A. Kheder, and M. F. Mimouni, "The wind energy conversion system using PMSG controlled by vector control and SMC strategies," *International Journal of Renewable Energy Research*, vol. 3, no. 1, pp. 41–50, 2013, <https://dergipark.org.tr/en/pub/ijrer/issue/16080/168268>.
- [52] M. Yin, G. Li, M. Zhou, and C. Zhao, "Modeling of the Wind Turbine with a Permanent Magnet Synchronous Generator for Integration," *2007 IEEE Power Engineering Society General Meeting*, pp. 1–6, 2007, <https://doi.org/10.1109/PES.2007.385982>.
- [53] N. K. Jena, K. B. Mohanty, H. Pradhan, and S. K. Sanyal, "A decoupled control strategy for a grid connected direct-drive PMSG based variable speed wind turbine system," *2015 International Conference on Energy, Power and Environment: Towards Sustainable Growth (ICEPE)*, pp. 1–6, 2015, <https://doi.org/10.1109/EPETSG.2015.7510098>.
- [54] P. Gajewski and K. Pieńkowski, "Advanced control of direct-driven PMSG generator in wind turbine system," *Arch. Electr. Eng.*, vol. 65, no. 4, pp. 643–656, 2016, <https://doi.org/10.1515/ae-2016-0045>.
- [55] L. Guo, X. Zhang, S. Yang, Z. Xie, L. Wang, and R. Cao, "Simplified model predictive direct torque control method without weighting factors for permanent magnet synchronous generator-based wind power system," *IET Electric Power Applications*, vol. 11, no. 5, pp. 793–804, 2016, <https://doi.org/10.1049/iet-epa.2015.0620>.
- [56] I. Jlassi and A. J. M. Cardoso, "Enhanced and Computationally Efficient Model Predictive Flux and Power Control of PMSG Drives for Wind Turbine Applications," in *IEEE Transactions on Industrial Electronics*, vol. 68, no. 8, pp. 6574–6583, Aug. 2021, <https://doi.org/10.1109/TIE.2020.3005095>.
- [57] M. Abdelrahem, C. Hackl, and R. Kennel, "Robust predictive control scheme for permanent-magnet synchronous generators based modern wind turbines," *Electronics*, vol. 10, no. 13, pp. 1–18, 2021, <https://doi.org/10.3390/electronics10131596>.